

Smooth extremal horizons are the exception, not the rule

Gary T. Horowitz¹ and Jorge E. Santos²

¹*Department of Physics, University of California, Santa Barbara, CA 93106, U.S.A.*

²*DAMTP, Centre for Mathematical Sciences, University of Cambridge, Wilberforce Road,
Cambridge CB3 0WA, UK*

horowitz@ucsb.edu, jss55@cam.ac.uk

ABSTRACT: We show that the general charged, rotating black hole in five-dimensional Einstein-Maxwell theory has a singular extremal limit. Only the known analytic solutions with exactly zero charge or zero angular momenta have smooth extremal horizons. When the two angular momenta are not equal and both are scaled to zero, the solution approaches a new family of static, nonspherical extremal black holes. We also consider general black holes in five-dimensional Einstein-Maxwell-Chern-Simons theory, and show that they also have singular extremal limits except for one special value of the coefficient of the Chern-Simons term (the one fixed by supergravity). Combining this with earlier results showing that extremal black holes have singular horizons in four-dimensional general relativity with small higher derivative corrections, and in anti-de Sitter space with perturbed boundary conditions, one sees that smooth extremal horizons are indeed the exception and not the rule.

Contents

1	Introduction	1
2	5D Einstein-Maxwell theory with possible Chern-Simons term	4
3	Near-horizon geometries	6
3.1	Perturbative in the angular momenta	8
3.2	Perturbative in the charge	11
3.3	Fully nonlinear results	13
4	Scaling dimensions	15
4.1	Perturbative in the angular momenta	16
4.2	Perturbative in the charge	21
4.3	Fully nonlinear results	24
5	Near extremal black holes	28
5.1	Numerical method	28
5.2	Results	32
6	Discussion	37
A	Scaling dimensions of the $U(1) \times U(1)$ symmetric near-horizon geometries	39
B	The scaling dimensions of the near-horizon geometries of extremal Myers-Perry black holes	40

1 Introduction

The five-dimensional (5D) generalization of the Kerr-Newman solution, describing charged rotating black holes, is not known. The 5D solution should contain four parameters: a mass M , charge Q , and two angular momenta, J_ϕ, J_ψ , corresponding to rotations in two orthogonal planes. Exact solutions to the 5D Einstein-Maxwell equations are known only when some of these parameters vanish. When $J_\phi = J_\psi = 0$, one has the static 5D generalization of the Reissner-Nordström solution [1], and when $Q = 0$, one has the vacuum Myers-Perry solutions [2]. Both of these solutions have smooth extremal limits (when J_ϕ, J_ψ are both nonzero). If one adds a Chern-Simons term to the action with its coefficient fixed by supergravity, the

general four-parameter family of black hole solutions is known [3], and again has smooth extremal limits. Given these results, one is tempted to conclude that the generic 5D (spherical¹) rotating charged black hole will have a smooth extremal limit.

The goal of this paper is to show that this intuition is completely wrong. We will show that generic 5D black holes have singular extremal limits. More precisely, black hole solutions to the 5D Einstein-Maxwell equations with nonzero Q, J_ϕ, J_ψ develop curvature singularities on their horizon in the extremal limit. This is probably why, despite considerable effort over the decades since the Myers-Perry solution was discovered (see [4] for a recent discussion), no one has found its charged generalization analytically. If one adds a Chern-Simons term with a coefficient λ normalised so that $\lambda = 1$ is the supergravity value, then extremal black holes remain singular as one increases λ , except for the precise value $\lambda = 1$. We find it remarkable that by studying black holes in a theory without fermions, one can select the value of λ required by supersymmetry. General relativity seems to know about supergravity.

There are two different types of curvature singularities that can arise depending on the parameters. For $|\lambda| < 1$, generic extremal black holes have diverging tidal forces and diverging electric fields for infalling observers as they approach the horizon. However, all scalars constructed from the curvature and Maxwell field do not blow up and remain finite. This is directly analogous to the singularities that are found for extremal black holes in four dimensions when small higher curvature corrections are added to general relativity [5, 6]. Similar singularities are found for extremal black holes in 4D anti-de Sitter space with perturbed boundary conditions [7]. The remarkable thing about five dimensions is that the generic extremal black hole is singular even in the simplest Einstein-Maxwell theory, without higher derivative corrections or perturbed boundary conditions.

When $|\lambda| > 1$, the singularity becomes stronger, and curvature scalars do blow up. We also find that for all λ , if one of the angular momenta vanish, then the extremal limit is singular in this strong sense. This is a well known property of 5D Myers-Perry black holes, but we will see that it continues to hold when any charge is added. In particular, if one adds an arbitrarily small amount of angular momentum in one plane to a 5D Reissner-Nordström black hole, the extremal horizon has diverging curvature scalars.

When the curvature scalars remain finite, the metric and vector potential are C^0 but not C^1 at the extremal horizon. Since the horizon becomes infinitely far away in spacelike directions, one can define a near-horizon geometry. When $Q \rightarrow 0$, it approaches the Myers-Perry near-horizon geometry. It is natural to expect that when the angular momenta vanish, it will approach the 5D Reissner-Nordström near-horizon geometry. However this is incorrect. We find that the solution approaches the more general static $U(1) \times U(1)$ symmetric near-horizon geometries [8] when J_ϕ and J_ψ both vanish. These metrics involve a squashed S^3 , and were originally interpreted as the near-horizon geometries of a nonrotating extremal black hole in a background electric field. We will show that the same geometries arise (without a background electric field) for an extremal black hole in the limit $J_\phi, J_\psi \rightarrow 0$, with the amount

¹We will consider only (asymptotically flat) black holes with horizon topology S^3 .

of squashing determined by the ratio J_ϕ/J_ψ . This implies that there are static, asymptotically flat extremal black holes that are not spherically symmetric!

These near-horizon geometries are smooth, but the exact metrics differ from them by a term than can be written $\rho^\gamma h$ where ρ is an affine distance to the horizon, h is a smooth tensor field, and the scaling dimension, γ , is determined by the field equations. We will show that for $|\lambda| < 1$, γ is not an integer and lies in the range $0 < \gamma < 1/2$, except for a couple of special cases (corresponding to the known analytic solutions). Similarly, the vector potential has power law behavior near the horizon with the same exponent. This is the origin of the diverging tidal forces and diverging electric fields for observers crossing the extremal horizon. Even though curvature scalars remain finite, this singularity is strong enough that Einstein's equation cannot be defined even in a distributional sense. For larger coefficients of the Chern-Simons term ($|\lambda| > 1$), curvature scalars diverge and there is no near-horizon geometry.²

We do not obtain these results by finding the general 5D rotating charged black hole solution explicitly. Even the general near-horizon geometry is not known analytically. Instead, we use a combination of numerical and perturbative arguments to establish our results. For example, in the case of pure Einstein-Maxwell theory, we start with the Myers-Perry near-horizon geometry and add charge perturbatively. We find that the black hole entropy does not depend on the charge and is given by³

$$S_1 = 2\pi \sqrt{|J_\phi J_\psi|}. \quad (1.1)$$

We also start with the general static $U(1) \times U(1)$ symmetric near-horizon geometry and add angular momenta perturbatively. The entropy is then given by

$$S_2 = \frac{4\sqrt{\pi}}{3^{3/4}} |Q|^{3/2} + \frac{3^{3/4}\pi^{3/2}}{4} \frac{|J_\phi J_\psi|}{|Q|^{3/2}} \quad (1.2)$$

Although this is initially derived just for small angular momenta, when we numerically compute the general near-horizon geometry, we find that it holds exactly for all angular momenta until $S_1 = S_2$. This occurs when

$$|J_\phi J_\psi| = \frac{16}{3\sqrt{3}\pi} |Q|^3 \quad (1.3)$$

When $|J_\phi J_\psi|$ exceeds this bound, the entropy is given by (1.1) exactly. So there are two branches of near-horizon geometries (when $\lambda = 0$) which meet at (1.3). The fact that these two branches have simple entropy formulas strongly suggests that there is an analytic solution for the general near-horizon geometry in this case. Finding this solution explicitly remains an open problem. In the special case $J_\phi = J_\psi$, there is enhanced symmetry and the analytic solution is known [9]. Our entropy formulas (1.1) and (1.2) reduce to the known expressions in this case.

²Strictly speaking, there is a solution with the symmetries of a near-horizon geometry, but it does not arise in the asymptotically flat solution.

³We set $G_5 = 1$ throughout this paper.

After finding the near-horizon geometries of the extremal solutions, we compute the scaling dimensions γ . We again first do this perturbatively for small charge and small angular momenta, and then compute γ numerically for the general case. Finally, we numerically construct the full asymptotically flat, near extremal solutions and show that the horizon becomes singular as one approaches extremality.

In the next section we introduce the one parameter family of 5D theories that we will consider, labelled by the coefficient of a Chern-Simons term. In section 3 we solve the field equations to determine the near-horizon geometries. The scaling dimensions are computed in Section 4, and the full asymptotically flat solutions are constructed in Section 5. Section 6 contains some discussion of these results, and the Appendices compute some of the higher scaling dimensions of the near-horizon geometries with zero charge or zero angular momenta.

2 5D Einstein-Maxwell theory with possible Chern-Simons term

We start with the following action

$$S = \frac{1}{16\pi} \int_{\mathcal{M}} d^5x \sqrt{-g} \left(R - \frac{1}{4} F^{ab} F_{ab} - \frac{\lambda}{12\sqrt{3}} \varepsilon^{abcde} F_{ab} F_{cd} A_e \right), \quad (2.1)$$

where R is the Ricci scalar associated with g , $F = dA$ is the Maxwell field strength, A is its gauge potential, and λ is a parameter that we take to be real. For $\lambda = 1$, the action above admits a supersymmetric completion, becoming the bosonic sector of minimal supergravity in five dimensions.

The equations of motion derived from the action (2.1) are:

$$R_{ab} - \frac{R}{2} g_{ab} = \frac{1}{2} \left(F_a{}^c F_{bc} - \frac{g_{ab}}{4} F^{cd} F_{cd} \right) \quad \text{and} \quad \nabla_b F^{ba} = \frac{\lambda}{4\sqrt{3}} \varepsilon^{abcde} F_{bc} F_{de}. \quad (2.2)$$

We are interested in constructing stationary and asymptotically flat black hole solutions to the above equations of motion. Furthermore, we focus on solutions that have a spatial $U(1)^2$ symmetry in addition to the timelike symmetry \mathbb{R} , with each of the $U(1)$ factors parametrisng rotations around a two-dimensional axis.

Let $k = \partial/\partial t$ be the stationary Killing vector field, normalised so that $k^2 = -1$ near null infinity. Additionally, let $m_\phi = \partial/\partial\phi$ generate a one-parameter group of isometries isomorphic to one of the $U(1)$ factors, and similarly for $m_\psi = \partial/\partial\psi$, with both $\phi \sim \phi + 2\pi$ and $\psi \sim \psi + 2\pi$.

For such solutions, one can compute their energy M , angular momenta J_ϕ and J_ψ and charge Q via Komar integrals [10] evaluated at spatial infinity as

$$M = \frac{3}{32\pi} \lim_{r \rightarrow +\infty} \int_{S_r^3} \star dk, \quad (2.3a)$$

$$J_\phi = -\frac{1}{16\pi} \lim_{r \rightarrow +\infty} \int_{S_r^3} \star dm_\phi, \quad (2.3b)$$

$$J_\psi = -\frac{1}{16\pi} \lim_{r \rightarrow +\infty} \int_{S_r^3} \star dm_\psi, \quad (2.3c)$$

and

$$Q = \frac{1}{16\pi} \int_\Sigma \left(\star F + \frac{\lambda}{\sqrt{3}} F \wedge A \right). \quad (2.3d)$$

where r is the standard radial coordinate near spatial infinity, and Σ is any (topological) three-sphere surrounding the black hole.

Note that there are several possible definitions of charge, due to the presence of the Chern-Simons term. Here we use the so called Page charge [11], which satisfies a Gauss law, making the result independent of the choice of integration surface Σ . One might worry that the Page charge is gauge dependent (since it explicitly depends on A). However, the gauge ambiguity can be fixed by demanding regularity of the vector field at the horizon, which we will assume henceforth.

Similarly, the angular momenta Komar integrals can be recast as integrals over a surface Σ , provided that Σ is a (topological) three-sphere surrounding the black hole. For vacuum spacetimes this can be done trivially, since $R_{ab} = 0$ implies that the integral does not change when one deforms the surface of integration. However this is not the case for the theory at hand. Indeed, there are matter contributions that must be included. After some algebra, one finds [12, 13]

$$J_\phi = -\frac{1}{16\pi} \int_\Sigma \left[\star dm_\phi + (m_\phi \cdot A) \star F + \frac{2\lambda}{3\sqrt{3}} (m_\phi \cdot A) A \wedge F \right], \quad (2.4)$$

and similarly for J_ψ . This expression can be used to read off the angular momenta of any black hole solution directly at the horizon and it will be of great help to interpret the integration constants when studying near-horizon geometries. Indeed, a similar expression also exists for the energy M .

We focus on black hole solutions satisfying Hawking's rigidity theorem [14] for which the event horizon H is a Killing horizon with the horizon generator being

$$K = k + \Omega_\phi m_\phi + \Omega_\psi m_\psi \quad (2.5)$$

with Ω_ϕ and Ω_ψ being constant [15] and interpreted as the black hole angular velocity along the ϕ and ψ angular directions. Furthermore, throughout, we will assume that spatial horizon cross sections have topology S^3 and that a bifurcating Killing three-sphere \mathcal{B}^+ exists where $K = 0$.

To the Killing horizon we can associate a constant [14] Hawking temperature [16],

$$T = \frac{1}{2\pi} \sqrt{-\frac{1}{4} \frac{\nabla_a (K^c K_c) \nabla^a (K^d K_d)}{K^e K_e} \Big|_H}, \quad (2.6)$$

from which we note that extremal black holes have $T = 0$. Finally, we define the chemical potential of the black hole event horizon, by defining

$$\mu = K^a A_a|_H - \lim_{r \rightarrow +\infty} K^a A_a. \quad (2.7)$$

Note that we are assuming a gauge choice where the Maxwell potential is regular on H . This is achieved by choosing a gauge where $K^a A_a|_H = 0$, ensuring that only the last term contributes. This gauge can always be attained because the results of [14] can be used to show that μ is necessarily constant.

One can show that, with the definitions above, the solutions we are seeking to construct must satisfy the first law of black hole mechanics

$$\delta M = T \delta S + \Omega_\phi \delta J_\phi + \Omega_\psi \delta J_\psi + \mu \delta Q \quad (2.8a)$$

where

$$S = \frac{A}{4}, \quad (2.8b)$$

with A being the area of the bifurcating Killing three-sphere \mathcal{B}^+ .

3 Near-horizon geometries

In this section we construct rotating and electrically charged near-horizon geometries. It has been shown that spherical, near-horizon geometries with a $U(1) \times U(1)$ symmetry must also have a $SO(2, 1)$ symmetry [17], so we will impose this below. We can choose an angular coordinate $x \in [-1, 1]$ so that the most general line element compatible with these symmetries is

$$\begin{aligned} ds_{\text{NH}}^2 = & Q_1(x) \left(-\rho^2 dt^2 + \frac{d\rho^2}{\rho^2} \right) + \frac{Q_2(x) dx^2}{1-x^2} + (1-x^2) Q_3(x) (d\phi + \omega_\phi \rho dt)^2 \\ & + x^2 Q_4(x) [d\psi + \omega_\psi \rho dt + (1-x^2) Q_5(x) (d\phi + \omega_\phi \rho dt)]^2 \end{aligned} \quad (3.1a)$$

and

$$\begin{aligned} A_{\text{NH}} = & -Q_{\text{NH}} \rho dt + (1-x^2) Q_6(x) (d\phi + \omega_\phi \rho dt) \\ & + x^2 Q_7(x) [d\psi + \omega_\psi \rho dt + (1-x^2) Q_5(x) (d\phi + \omega_\phi \rho dt)] \end{aligned} \quad (3.1b)$$

Note that the first expression in parenthesis is just two-dimensional anti-de Sitter space. There are a total of seven functions of x to solve for, denoted $Q_I(x)$ where $I = 1, \dots, 7$. There are also three constants, ω_ϕ , ω_ψ and Q_{NH} , which will determine the angular momenta and charge of the solution. At this point, we have not yet chosen a specific gauge and are keeping the ansatz as general as possible, but consistent with a $O(2, 1) \times U(1)_\phi \times U(1)_\psi$ symmetry.

Note that regularity at $x = 1$, the axis of the ϕ rotation, demands that

$$Q_2(1) = Q_3(1) \quad (3.2a)$$

while regularity at $x = 0$, the axis of the ψ rotation, demands that

$$Q_2(0) = Q_4(0) \quad (3.2b)$$

For $\lambda = 1$, analytic solutions are known to exist, with the most general being the near-horizon limit of a particular extremal family of solutions found in [18]⁴. These have

$$\omega_\phi = \frac{a_\psi (a_\phi + a_\psi)^2 + (a_\phi + 2a_\psi) q}{2\sqrt{a_\phi a_\psi + q} [(a_\phi + a_\psi)^2 + q]}, \quad \omega_\psi = \frac{a_\phi (a_\phi + a_\psi)^2 + (2a_\phi + a_\psi) q}{2\sqrt{a_\phi a_\psi + q} [(a_\phi + a_\psi)^2 + q]},$$

$$\text{and } Q_{\text{NH}} = \frac{\sqrt{3}q^2}{2\sqrt{a_\phi a_\psi + q} [(a_\phi + a_\psi)^2 + q]}, \quad (3.3a)$$

with q , a_ϕ and a_ψ being constants that parametrise charge and rotations along the ϕ and ψ axis. Furthermore,

$$Q_2(x) = 4Q_1(x) = a_\phi a_\psi + q + a_\phi^2 x^2 + a_\psi^2 (1 - x^2) \quad (3.3b)$$

$$Q_3(x) = \frac{4(a_\phi a_\psi + q) [(a_\phi + a_\psi)^2 + q]^2 Q_1(x)}{Z(x)} \quad (3.3c)$$

$$Q_4(x) = \frac{Z(x)}{16Q_1(x)^2} \quad (3.3d)$$

$$Q_5(x) = \frac{4(a_\phi + b_\psi)^2 (a_\phi b_\psi + q) Q_1(x) - a_\phi b_\psi q^2}{Z(x)} \quad (3.3e)$$

$$Q_6(x) = -\frac{\sqrt{3}q}{Z(x)} \{4(a_\phi + a_\psi) (a_\phi a_\psi + q) Q_1(x) - a_\psi q [a_\psi (a_\phi + a_\psi) + q]\} \quad (3.3f)$$

$$Q_7(x) = -\frac{\sqrt{3}a_\psi q}{4Q_1(x)}, \quad (3.3g)$$

where

$$Z(x) = [a_\psi (a_\phi + a_\psi) + q]^3 + (a_\phi - a_\psi) (a_\phi + a_\psi)^3 (a_\phi a_\psi + q) x^4$$

$$+ \left[(2a_\phi - a_\psi) a_\psi^2 (a_\phi + a_\psi)^3 + (4a_\phi - a_\psi) a_\psi (a_\phi + a_\psi)^2 q + (2a_\phi^2 + 2a_\phi a_\psi - a_\psi^2) q^2 \right] x^2. \quad (3.3h)$$

For $a_\phi = a_\psi = 0$, we recover the standard near-horizon geometry of a Reissner-Nordström black hole, while for $q = 0$, we have the near-horizon geometry of an extremal Myers-Perry black hole in five spacetime dimensions [2]. For both of these particular cases, the above solution is valid for *any* value of λ .

We aim to investigate whether *smooth* solutions exist for $\lambda \neq 1$ and generic values of the charge and angular momenta. This will be done in three steps. First, we will take the limit of small angular momenta, where perturbation theory can be applied to proceed analytically. Similarly, we will study the small charge limit analytically. Finally, we will numerically construct typical near-horizon geometries for generic values of the angular momenta and charge.

⁴This general solution contains extra fields coming from string theory. We restrict our attention to the particular solution presented in [3], and set the cosmological constant to zero.

3.1 Perturbative in the angular momenta

To find the near-horizon geometry with slow rotation, it is natural to try to perturb the near-horizon geometry of 5D Reissner-Nordström. However, one soon encounters an obstruction. To obtain a perturbative solution, one must start with the most general static near-horizon geometry in Einstein-Maxwell-Chern-Simons theory (with vanishing magnetic field), possessing $O(2,1) \times U(1)_\phi \times U(1)_\psi$ isometry, as found in [8]:

$$ds_{\text{NH}}^2 = \Gamma(x) \left(-\rho^2 dT^2 + \frac{d\rho^2}{\rho^2} \right) + \frac{\sigma(x)^2 dx^2}{1-x^2} + \frac{c_2^3}{\sigma(x)} (1-x^2) d\phi^2 + \frac{c_1^3}{\sigma(x)} x^2 d\psi^2 \quad (3.4a)$$

and

$$A = -\frac{\sqrt{3c_1c_2}}{2} \rho dT \quad (3.4b)$$

with

$$\sigma(x) = c_1(1-x^2) + c_2x^2, \quad \Gamma(x) = \sigma(x)^2/4 \quad (3.5)$$

where both c_1 and c_2 are positive real constants that describe the size and squashing of an S^3 . When $c_1 = c_2$ the sphere is round and the solution reduces to the near-horizon geometry of an extremal 5D Reissner-Nordström black hole.

To account for the effects of rotation, we modify the above expression accordingly and set:

$$ds_{\text{NH}}^2 = \Gamma(x) \left(-\rho^2 dT^2 + \frac{d\rho^2}{\rho^2} \right) + \frac{\sigma_1(x)\sigma_2(x)dx^2}{1-x^2} + \frac{B_2}{\sigma_1(x)} (1-x^2) (d\phi + \Omega_\phi \rho dT)^2 \\ + \frac{B_1}{\sigma_2(x)} x^2 [d\psi + \Omega_\psi \rho dT + (1-x^2)\alpha(x) (d\phi + \Omega_\phi \rho dT)]^2 \quad (3.6a)$$

and

$$A = -Q_H \rho dT + \beta(x)(1-x^2) (d\phi + \Omega_\phi \rho dT) \\ + \delta(x)x^2 [d\psi + \Omega_\psi \rho dT + (1-x^2)\alpha(x) (d\phi + \Omega_\phi \rho dT)] . \quad (3.6b)$$

Here, B_1 and B_2 are constants that will be adjusted within perturbation theory to eliminate any conical singularities, while Ω_ϕ and Ω_ψ are real constants that parameterize rotation along the ϕ and ψ directions, respectively. There are now six functions of x to solve for: $\Gamma(x)$, $\sigma_1(x)$, $\sigma_2(x)$, $\alpha(x)$, $\beta(x)$, and $\delta(x)$. Note that, since the equations of motion are invariant under the rescalings $g \rightarrow \hat{\lambda}^2 g$ and $A \rightarrow \hat{\lambda} A$, with $\hat{\lambda}$ an arbitrary constant, we can always choose Q_H such that

$$Q_H = \frac{\sqrt{3c_1c_2}}{2} . \quad (3.7)$$

We have fixed the gauge such that the determinant of a spatial cross-section of the extremal horizon is simply given by $x\sqrt{B_1B_2}$. In these coordinates, we are left with six coupled differential equations for Γ , σ_1 , σ_2 , α , β , and δ , five of which are second-order in x , and one is first-order.

We are now ready to establish our perturbative scheme. Pick two constants, ω_ϕ and ω_ψ , to describe the rotations we are adding, and define

$$\Omega_\phi = \varepsilon \omega_\phi, \quad \Omega_\psi = \varepsilon \omega_\psi \quad (3.8)$$

and set

$$\begin{aligned} \Gamma(x) &= \frac{\sigma(x)^2}{4} \left[1 + \sum_{i=1}^{+\infty} \varepsilon^{2i} \Gamma^{(2i)}(x) \right], \quad \alpha(x) = \sum_{i=1}^{+\infty} \varepsilon^{2i} \alpha^{(2i)}(x) \\ B_I &= c_I^3 \left[1 + \sum_{i=1}^{+\infty} \varepsilon^{2i} B_I^{(2i)} \right], \quad \sigma_I(x) = \sigma(x) \left[1 + \sum_{i=1}^{+\infty} \varepsilon^{2i} \sigma_I^{(2i)}(x) \right] \quad \text{with } I = 1, 2, \\ \beta(x) &= \sum_{i=0}^{+\infty} \varepsilon^{2i+1} \beta^{(2i+1)}(x) \quad \text{and} \quad \delta(x) = \sum_{i=0}^{+\infty} \varepsilon^{2i+1} \delta^{(2i+1)}(x), \end{aligned} \quad (3.9)$$

while taking ε to be arbitrarily small. Note that the introduction of Ω_ϕ and Ω_ψ sources first order perturbations to the vector potential but only second order perturbations to the metric functions.

At zeroth order we recover Eqs. (3.4), At linear order we find

$$\begin{aligned} \beta^{(1)}(x) &= -\frac{2\sqrt{3c_2} (c_2^2 \omega_\phi - 2\lambda c_1^2 \omega_\psi)}{(1 - 4\lambda^2) \sqrt{c_1} \sigma(x)} + \frac{\Omega_1}{1 - x^2} + \frac{\lambda Z(x)}{1 - x^2}, \\ \delta^{(1)}(x) &= -\frac{2\sqrt{3c_1} (c_1^2 \omega_\psi - 2\lambda c_2^2 \omega_\phi)}{(1 - 4\lambda^2) \sqrt{c_2} \sigma(x)} + \frac{\Omega_2}{x^2} + \frac{c_1 \sigma(x) Z'(x)}{4x c_2^2}, \\ Z(x) &= x^{4\lambda} \sigma(x)^{-2\lambda} \Omega_3 {}_2F_1 \left(-2\lambda, -2\lambda; 1 - 4\lambda; \frac{\sigma(x)}{x^2 c_2} \right) \\ &\quad + x^{-4\lambda} \sigma(x)^{2\lambda} \Omega_4 {}_2F_1 \left(2\lambda, 2\lambda; 1 + 4\lambda; \frac{\sigma(x)}{x^2 c_2} \right), \end{aligned} \quad (3.10)$$

where ${}_2F_1(a, b; c; z)$ is a Gauss hypergeometric function, and Ω_i , $i = 1, \dots, 4$ are constant coefficients. Regularity requires $\Omega_1 = \Omega_2 = 0$. In addition, if $\lambda \geq 0$, then $\Omega_4 = 0$ and if $\lambda \leq 0$, then $\Omega_3 = 0$. Finally, if 2λ is not an integer, regularity requires both $\Omega_3 = \Omega_4 = 0$ so $Z(x)$ vanishes. For $\lambda = 1/2$ or $\lambda = 1$, $Z(x)$ can be nontrivial, and in particular

$$Z(x) = -\frac{c_1 (1 - x^2)}{c_2 \sigma(x)} \Omega_3 \quad \text{for } \lambda = 1/2 \quad (3.11a)$$

$$Z(x) = \frac{c_1 (1 - x^2)}{3c_2^2 \sigma(x)^2} [c_1 (1 - x^2) - 2c_2 x^2] \Omega_3 \quad \text{for } \lambda = 1. \quad (3.11b)$$

Our conclusions remain the same if we take 2λ to be a non-zero integer, but for clarity, we will assume otherwise in this presentation. Without loss of generality, we will also assume $\lambda \geq 0$.

We now move to second order perturbation theory in ε . At second order we find that $\alpha^{(2)}$ obeys a second order differential equation that we can readily solve while imposing the

relevant boundary conditions

$$\alpha^{(2)}(x) = \frac{4c_1}{(1 - 4\lambda^2)^2 \sigma(x)} [3\lambda (\hat{\alpha}^4 \omega_\phi^2 + \omega_\psi^2) - \hat{\alpha}^2 (1 + 10\lambda^2 - 8\lambda^4) \omega_\psi \omega_\phi] \quad (3.12)$$

with $\hat{\alpha} \equiv c_2/c_1$. Finally, $\Gamma^{(2)}$, $\sigma_1^{(2)}$, and $\sigma_2^{(2)}$ satisfy three coupled ordinary differential equations. To solve these, we introduce two auxiliary variables, \mathfrak{a}_1 and \mathfrak{a}_2 , defined as follows:

$$\Gamma^{(2)}(x) = \mathfrak{a}_1(x) \quad \text{and} \quad \sigma_1^{(2)}(x) = \mathfrak{a}_2(x) - \sigma_2^{(2)}(x). \quad (3.13)$$

As a result of this substitution, $\mathfrak{a}_1(x)$ and $\mathfrak{a}_2(x)$ decouple from $\sigma_2^{(2)}(x)$, which now satisfies a first-order differential equation driven by $\mathfrak{a}_1(x)$, $\mathfrak{a}_2(x)$, and their first derivatives. We are left with two second-order differential equations for $\mathfrak{a}_1(x)$ and $\mathfrak{a}_2(x)$. It turns out that these last two equations can be solved in full generality. We will refrain from presenting these solutions explicitly. The general solutions for $\mathfrak{a}_1(x)$ and $\mathfrak{a}_2(x)$ depend on four integration constants, and we have not yet imposed any regularity conditions. Therefore, we can solve for $\sigma_2^{(2)}(x)$ in full generality, though this introduces an additional integration constant. In total, the general solution for $\Gamma^{(2)}(x)$, $\sigma_1^{(2)}$, and $\sigma_2^{(2)}$ depends on five integration constants. The final step involves requiring these functions to remain regular at the poles $x = 0$ and $x = 1$. This procedure fixes three of the integration constants *and* demands that

$$\omega_\phi = \pm \frac{c_1^2}{c_2^2} \omega_\psi. \quad (3.14)$$

We will consider only the upper sign, as we assume that both angular momenta are positive. The analysis for opposite sign angular momenta can be repeated *mutatis mutandis*. This last expression justifies why we had to take Eqs. (3.4) as our background. Indeed, to ensure that the angular momenta can be different from each other, we need to consider cases where $c_1 \neq c_2$ and the S^3 is squashed! This also shows that if we try to add rotation in only one plane and set the other to zero, the sphere becomes infinitely squashed and hence singular.

Finally, we could now adjust $B_1^{(2)}$ and $B_2^{(2)}$ to remove any hypothetical conical singularity at $x = 0$ and $x = 1$, respectively. Once the procedure outlined above is done, it is a simple matter to compute the entropy, charge and angular momenta of the new near-horizon geometries. These combine in the following simple result

$$\frac{S}{|Q|^{3/2}} = \frac{4\sqrt{\pi}}{3^{3/4}} + \frac{3^{3/4}\pi^{3/2}(1 + 2\lambda)}{2(2 + \lambda)} \frac{J_\phi J_\psi}{|Q|^3} + \mathcal{O}(\epsilon^3) \quad (3.15)$$

The above expression was derived using perturbation theory. However, for $\lambda = 0$, it turns out to yield the full nonlinear result (with no $\mathcal{O}(\epsilon^3)$ correction). At this point, we have no justification for why this is the case, as we only know the geometry perturbatively. However, when comparing with the full numerical results in the next sections, we find that the above expression for $\lambda = 0$ agrees with the full nonlinear results to the first twenty decimal places, even when J_ϕ and J_ψ are of the same order as $Q^{3/2}$. This agreement is exact only for $\lambda = 0$.

Indeed, using the known analytic solution with $\lambda = 1$ (see Eqs. (3.3)), it is a straightforward exercise to show that the expression for $\frac{S}{|Q|^{3/2}}$ given above is valid only to leading order in J_ϕ and J_ψ . The above result assumed $J_\phi J_\psi \geq 0$. When $J_\phi J_\psi < 0$, we get instead that

$$\frac{S}{|Q|^{3/2}} = \frac{4\sqrt{\pi}}{3^{3/4}} - \frac{3^{3/4}\pi^{3/2}(1-2\lambda)}{2(2-\lambda)} \frac{J_\phi J_\psi}{|Q|^3} + \mathcal{O}(\epsilon^3). \quad (3.16)$$

3.2 Perturbative in the charge

Introducing charge perturbatively is considerably more cumbersome than introducing angular momenta perturbatively. The reason is that the starting point, namely the five-dimensional extreme Myers-Perry solution, is more intricate than the general $U(1) \times U(1)$ static near-horizon geometry given in Eqs. (3.4).

We change gauge and set

$$ds^2 = \Gamma(x) \left\{ -\rho^2 dT^2 + \frac{d\rho^2}{\rho^2} + \frac{\Gamma_{\text{NH}}^2 dx^2}{1-x^2} + h_{11}(x)(1-x^2)(d\phi + \Omega_\phi \rho dT)^2 \right. \\ \left. + h_{22}(x)x^2 [d\psi + \Omega_\psi \rho dT + (1-x^2)h_{12}(x)(d\phi + \Omega_\phi \rho dT)]^2 \right\}, \quad (3.17a)$$

$$A = -Q_{\text{NH}} dT + b_1(x)(1-x^2)(d\phi + \Omega_\phi \rho dT) \\ + b_2(x)x^2 [d\psi + \Omega_\psi \rho dT + (1-x^2)h_{12}(x)(d\phi + \Omega_\phi \rho dT)] , \quad (3.17b)$$

with Γ_{NH} and Q_{NH} real constants to be determined in what follows. Note that in these coordinates, the coefficients of dx^2 and $d\rho^2$ are related in a simpler manner than in our previous ansatz Eq (3.6). At the nonlinear level we are left with six second order differential equations in x for h_{11} , h_{12} , h_{22} , Γ , b_1 and b_2 and one nonlinear constraint quadratic in the first derivatives of h_{11} , h_{12} , h_{22} , Γ , b_1 and b_2 . The absence of conical singularities at $x = 0$ and $x = 1$ demand

$$\Gamma_{\text{NH}}^2 = h_{22}(0) \quad \text{and} \quad \Gamma_{\text{NH}}^2 = h_{11}(1) \quad (3.18)$$

respectively.

Our background is simply a five-dimensional extremal Myers-Perry black hole, for which

$$\Gamma(x) = \Gamma^{(0)}(x) = \frac{1}{4}(a+b) [ax^2 + b(1-x^2)] \quad (3.19a)$$

$$h_{11}(x) = h_{11}^{(0)}(x) = \frac{4a(a+b)}{(b+ax^2)[ax^2 + b(1-x^2)]} \quad (3.19b)$$

$$h_{12}(x) = h_{12}^{(0)} = \frac{a}{b+ax^2} \quad (3.19c)$$

$$h_{22}(x) = h_{22}^{(0)} = \frac{4b(b+ax^2)}{[ax^2 + b(1-x^2)]^2} \quad (3.19d)$$

$$\Gamma_{\text{NH}} = 2 \quad (3.19\text{e})$$

$$\Omega_\phi = \frac{1}{2}\sqrt{\frac{b}{a}} \quad \text{and} \quad \Omega_\psi = \Omega_\psi^{(0)} = \frac{1}{2}\sqrt{\frac{a}{b}} = \frac{1}{4\Omega_\phi} \quad (3.19\text{f})$$

while b_1 , b_2 and Q_{NH} vanish. Rather than label the solutions by the rotation parameters (a, b) , perturbation theory will be easier to present if we label them by (a, Ω_ϕ) using $b = 4a\Omega_\phi^2$. In the near-horizon geometry of an extremal Myers-Perry black hole, Ω_ψ is then fixed by $4\Omega_\psi\Omega_\phi = 1$.

Our perturbation scheme reads

$$\begin{aligned} \Omega_\psi &= \sum_{i=0}^{+\infty} q^i \Omega_\psi^{(i)}, \quad Q_{\text{NH}} = \sum_{i=1}^{+\infty} q^i Q_{\text{NH}}^{(i)}, \quad \Gamma(x) = \sum_{i=0}^{+\infty} q^i \Gamma^{(i)}(x), \\ h_{IJ}(x) &= \sum_{i=0}^{+\infty} q^i h_{IJ}^{(i)}(x), \quad \text{and} \quad b_I(x) = \sum_{i=1}^{+\infty} q^i b_I^{(i)}(x) \quad \text{with} \quad I, J = 1, 2, \end{aligned} \quad (3.20)$$

while maintaining $\Gamma_{\text{NH}} = 2$.

To zeroth order, we recover the near-horizon geometry of an extremal Myers-Perry black hole by construction. At linear order, the equations for the $b_I(x)$ decouple from the remainder and we find

$$b_1(x) = \frac{\varphi_0 + 4\Omega_\phi^2 \varphi_1}{x^2 + 4\Omega_\phi^2} \quad \text{and} \quad b_2(x) = \varphi_1 + \frac{4\Omega_\phi^2 \varphi_0}{x^2 + 4\Omega_\phi^2(1 - x^2)}, \quad (3.21)$$

with φ_0 and φ_1 integration constants. The equations for $\Gamma^{(1)}(x)$ and the $h_{IJ}^{(1)}(x)$ are coupled, but can be solved after the following field redefinition:

$$\begin{aligned} \Gamma^{(1)}(x) &= \tilde{\Gamma}^{(1)}(x) - \frac{a^2}{48} (x^2 + 4\Omega_\phi^2) [x^2 + 4\Omega_\phi^2 (1 - x^2)]^2 h_{11}^{(1)}(x) \\ &\quad - \frac{a^2 (1 + 4\Omega_\phi^2) [x^2 + 4\Omega_\phi^2 (1 - x^2)]^3}{192\Omega_\phi^2 (x^2 + 4\Omega_\phi^2)} h_{22}^{(1)}(x). \end{aligned} \quad (3.22)$$

We are left with a second order equation for $\tilde{\Gamma}^{(1)}(x)$ (which can be readily solved) and three equations for the $h_{IJ}^{(1)}(x)$, with two being second order and one being first order. These equations, in turn, can be solved analytically. The full solution at this order, and prior to imposing any boundary condition, depends on seven integration constants. Regularity conditions, including the absence of conical singularities, determine five of these integration constants along with:

$$Q_{\text{NH}}^{(1)} = 0. \quad (3.23)$$

Once we have determined the solution up to this order, we can readily compute all the corresponding charges, as well as the entropy. In fact, we carried out the above calculation to second order in q . Once the dust settles, we find

$$S = 2\pi \sqrt{|J_\phi J_\psi|} + \mathcal{O}(q^3). \quad (3.24)$$

Note that S , J_ϕ , and J_ψ are complicated functions of a , φ_0 , φ_1 , Ω_ϕ , and λ , yet the above expression still holds. Since the Chern-Simons term is cubic in the vector potential, it will only enter the analysis at $\mathcal{O}(q^3)$. However, if $\lambda = 0$, the exact numerical data described in the next section agrees with the above expression exactly (with no $\mathcal{O}(q^3)$ corrections)! In other words, the extremal entropy is independent of the charge. At the moment we have no understanding of why that is the case. Our results at small angular momenta, and small charge strongly suggest that, at least for $\lambda = 0$, an analytic solution interpolating between the static $U(1) \times U(1)$ near-horizon geometry and the near-horizon geometry of an extreme Myers-Perry black hole ought to exist.

3.3 Fully nonlinear results

To find the near-horizon geometry for generic values of the angular momenta, charge and λ we proceed numerically. We use the DeTurck trick, first proposed in [19] and reviewed in [20, 21]. We start with a generic line element and gauge field that are compatible with $O(2,1) \times U(1)_\phi \times U(1)_\psi$, as in Eqs. (3.1). Instead of solving the Einstein equation (2.2), we solve the Einstein-DeTurck equation:

$$R_{ab} - \nabla_{(a}\xi_{b)} = \frac{1}{2} \left(F_a{}^c F_{bc} - \frac{g_{ab}}{6} F^{cd} F_{cd} \right), \quad (3.25)$$

while leaving Maxwell's equation unchanged. If $\xi = 0$, the above reduces to the trace-reversed form of (2.2). The vector ξ is called the DeTurck vector and is defined as $\xi^a = [\Gamma_{bc}^a(g) - \Gamma_{bc}^a(\bar{g})] g^{bc}$, where $\Gamma_{bc}^a(\mathbf{g})$ are the components of the Levi-Civita connection associated with a metric \mathbf{g} . \bar{g} is the so-called reference metric, and essentially controls the gauge choice, as we will shortly see.

When $\xi = 0$, solutions of (3.25) coincide with those of the original Einstein equation (2.2). However, this is almost certainly not the case when $\xi \neq 0$. Solutions with $\xi \neq 0$ are called Ricci solitons, and when $F = 0$, they were shown not to exist when searching for certain stationary solutions [22]. In our case, such unphysical solutions can, in principle, exist. However, for stationary solutions like the ones we aim to construct, Eq. (3.25) leads to a system of elliptic partial differential equations, once appropriate boundary conditions are specified. Crucially, elliptic partial differential equations yield locally unique solutions. This implies that solutions with $\xi \neq 0$ cannot be arbitrarily close to those with $\xi = 0$. Therefore, once we find a solution, we can monitor $\xi^a \xi_a \geq 0$ and verify whether it approaches zero as we refine the resolution of our numerical scheme. Since we are solving the Einstein equation when $\xi^a = 0$, one might wonder which gauge this procedure naturally induces. We recall that $\xi^a = [\Gamma_{bc}^a(g) - \Gamma_{bc}^a(\bar{g})] g^{bc} = \square x^a - \tilde{S}^a$, where $\tilde{S}^a \equiv \Gamma_{bc}^a(\bar{g}) g^{bc}$. This indicates that the DeTurck gauge is essentially a stationary version of the usual generalized harmonic gauge.

We now turn our attention to boundary conditions for the functions in (3.1). At $x = 0$, to avoid a conical singularity, we require that $Q_2(0) = Q_4(0)$, with the other functions being even across $x = 0$. At $x = 1$, however, we have $Q_2(1) = Q_3(1)$, while the remaining functions satisfy Robin boundary conditions, which we will refrain from presenting here.

It remains to specify what reference metric we take in our construction. For the problem at hand, we picked \bar{g} to be given by $4Q_1 = Q_2 = Q_3 = Q_4 = 4$ and $Q_5 = 0$ in Eqs. (3.1). To solve the Einstein-DeTurck and Maxwell's equations, we used spectral collocation methods on a Gauss-Lobatto grid with N collocation points. Once we have a given solution, we checked that as N increases, $\xi^a \xi_a$ approached zero exponentially fast in N . For all the plots shown in this section we used $N = 200$.

Our moduli space of solutions depends on the Chern-Simons coefficient λ , the angular momenta J_ϕ and J_ψ , and the electric charge Q . Using the scaling symmetry $g \rightarrow \hat{\lambda}^2 g$ and $F \rightarrow \hat{\lambda} F$, with $\hat{\lambda}$ a real constant, we can always rescale one of these quantities so that only the appropriately normalised ratios are meaningful. We will work with $J_\phi/|Q|^{3/2}$ and $J_\psi/|Q|^{3/2}$, demonstrating that for fixed λ , we have a continuous two-dimensional moduli space of solutions. In our numerical scheme we have access to Q_{NH} , ω_ϕ and ω_ψ , which we dial to move across the two-dimensional phase space of solutions

In Fig. 1, we plot $S/|Q|^{3/2}$ as a function of $J_\phi/|Q|^{3/2}$ for $J_\psi/J_\phi = 3/8$, with λ fixed at 0. (Other ratios of J_ψ/J_ϕ display qualitatively similar behavior.) The blue and orange curves describe our numerical solutions. For small angular momenta, we find a single family of solutions and the blue curve appears to follow Eq. (1.2) (denoted by a black dashed line) exactly. This indicates that our perturbative result for small angular momenta (3.15) does not receive any higher order corrections, and actually holds beyond the perturbative regime. For large angular momenta, we find two different families of solutions. The blue curve appears to follow Eq. (1.1) (denoted by a long-dashed gray line) exactly, indicating that our perturbative result for small charge (3.24) also does not receive corrections. The second branch of solutions, denoted by the orange curve, appears to follow a continuation of Eq. (1.2). It starts at the point where the two entropy formulas (1.1) and (1.2) agree, which occurs when

$$J_\phi J_\psi = \frac{16}{3\sqrt{3}\pi} Q^3 \quad (3.26)$$

This point is denoted by the red dot in Fig. 1. We will show in Sec. 4 that the orange branch of near-horizon geometries cannot be extended to asymptotically flat solutions. So only the blue curve represents extremal charged rotating black holes in 5D Einstein-Maxwell theory.

The picture above changes when we turn on λ . For any $\lambda \neq 0$, we find that Eq. (3.15) and Eq. (3.24) are only valid in the regimes where they were derived, i.e., for small angular momenta and small charge, respectively. Interestingly, we no longer observe a merger between distinct families of solutions. The two families of solutions represented by the blue and orange curves in Fig. 1 separate, and the kink in the blue curve at (3.26) smooths out. The orange curve stops above the blue curve, and connects to yet another family of solutions. However we will see that only the blue curve describes near-horizon geometries that connect to asymptotically flat regions.

We illustrate this behaviour in Fig. 2, which was constructed for fixed $\lambda = 0.01$. On the left panel we show the normalised entropy $S/|Q|^{3/2}$ as a function of the normalised angular momentum $J_\phi/|Q|^{3/2}$ for all the different branches found, while on the right panel we plot

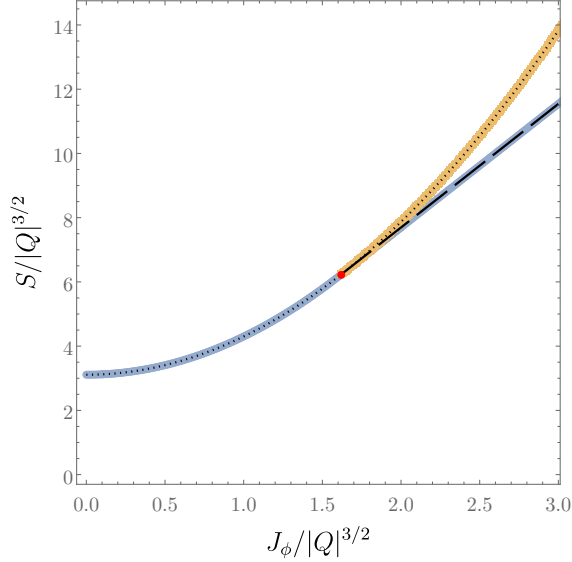


Figure 1. Normalised entropy $S/|Q|^{3/2}$ as a function of the normalised angular momentum $J_\phi/|Q|^{3/2}$ for fixed $J_\psi = 3J_\phi/8$ in 5D Einstein-Maxwell theory. To the left of the red dot, the blue curve satisfies Eq. (1.2), and to the right it satisfies Eq. (1.1). The orange branch corresponds to near-horizon geometries which do not extend to asymptotically flat solutions.

a blow-up of the region of angular momenta close to (3.26) (the red dot in Fig. 1). In both panels, the new branch of solutions is represented in green. This new branch does not appear to extend to arbitrarily large values of $J_\phi/|Q|^{3/2}$. The gap between the blue branch of solutions and the rest is clear on the right. The point where the orange and green branches of solutions merge moves to larger angular momenta as we increase λ . For instance, for $\lambda \approx 0.12$ this starting point is already above $J_\phi/|Q|^{3/2} = 3.7$ for fixed $J_\psi = 3J_\phi/8$, so the diagram on the left would show only the blue curve.

As we continue to increase λ , we eventually reach $\lambda = 1$, and the numerical curve coincides with

$$S = \sqrt{\left| \frac{16\pi}{3\sqrt{3}} Q^3 + 4\pi^2 J_\phi J_\psi \right|}, \quad (3.27)$$

which was computed directly from Eqs. (3.3), giving reassurance that our numerical code is correct.

4 Scaling dimensions

We now turn our attention to computing the scaling dimensions associated with our near-horizon geometries. Following the same strategy as in the previous section, we first perform the calculations analytically at small angular momenta and small charge, before proceeding to the fully nonlinear regime, which we once again explore using numerical methods.

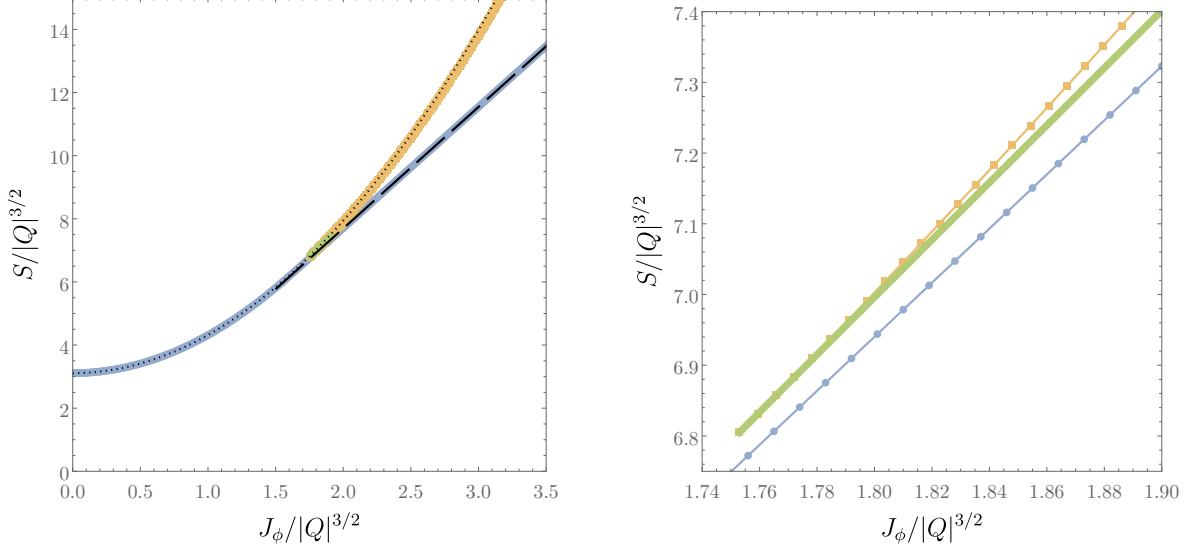


Figure 2. Left Panel: Normalised entropy $S/|Q|^{3/2}$ as a function of the normalised angular momentum $J_\phi/|Q|^{3/2}$ for fixed $J_\psi = 3J_\phi/8$ and $\lambda = 10^{-2}$. **Right Panel:** A blow-up of the center region of the left panel. Three distinct families of near-horizon geometries are visible, but only the one denoted by blue dots can be extended to asymptotically flat solutions.

4.1 Perturbative in the angular momenta

In this section we describe how to compute the scaling dimensions γ using perturbation theory about the static $U(1) \times U(1)$ symmetric near-horizon geometries described in Sec. 3.1 above. Our perturbatively small parameters will be the angular momenta J_ϕ and J_ψ as in that section. It was noted in [7] that the lowest scaling dimension associated with the near-horizon geometry of an extremal Reissner-Nordström black hole in 5D is $\gamma = 0$. This occurs when deformations in the near-horizon region are generated by an $\ell = 2$ harmonic mode on the three-sphere. Since adding rotation to a spherically symmetric spacetime involves vector spherical harmonics, we expect the backreaction of angular momenta on the geometry to alter the corresponding scaling dimensions at second order. We will show that there is a $\gamma = 0$ perturbation even when we deform the S^3 in the near-horizon geometry, and adding angular momenta indeed shifts γ above zero. When this happens, the horizon becomes singular since the metric is continuous but no longer differentiable there.

We will choose our gauge so that

$$\begin{aligned} ds^2 = & Q_1(x, \rho) \left(-\rho^2 dT^2 + \frac{d\rho^2}{\rho^2} \right) + \frac{Q_2(x, \rho) dx^2}{1 - x^2} + \frac{1 - x^2}{Q_3(x, \rho)} (d\phi + \rho Q_6(x, \rho) dT)^2 \\ & + \frac{x^2}{Q_4(x, \rho)} [d\psi + \rho Q_7(x, \rho) dT + (1 - x^2) Q_5(x, \rho) (d\phi + \rho Q_6(x, \rho) dT)]^2 \end{aligned} \quad (4.1a)$$

and

$$A = -\rho Q_8(x, \rho) dT + Q_9(x, \rho)(1 - x^2) (d\phi + \rho Q_6(x, \rho) dT) \\ + Q_{10}(x, \rho)x^2 [d\psi + \rho Q_7(x, \rho) dT + (1 - x^2)Q_5(x, \rho) (d\phi + \rho Q_6(x, \rho) dT)] , \quad (4.1b)$$

resulting in a total of ten functions Q_I of ρ and x to solve for. We compute the scaling dimensions by considering linearized deformations of the near-horizon geometries proportional to ρ^γ . A linearized approximation is sufficient since (for $\gamma > 0$) the deformation becomes very small near the horizon. Note that, in effect, we have a double expansion. We know the near-horizon geometries in an expansion in angular momenta, and for each order in that expansion, we compute γ by solving the equations for a linear deformation.

To compute the scaling dimensions we set

$$\begin{aligned} Q_1(x, \rho) &= \Gamma(x) (1 + \epsilon \rho^\gamma q_1(x)) \\ Q_2(x, \rho) &= \sigma_1(x)\sigma_2(x) (1 + \epsilon \rho^\gamma q_2(x)) \\ Q_3(x, \rho) &= \frac{\sigma_1(x)}{A_2} (1 + \epsilon \rho^\gamma q_3(x)) \\ Q_4(x, \rho) &= \frac{\sigma_2(x)}{A_1} (1 + \epsilon \rho^\gamma q_4(x)) \\ Q_5(x, \rho) &= \alpha(x) (1 + \epsilon \rho^\gamma q_5(x)) \\ Q_6(x, \rho) &= \Omega_\phi (1 + \epsilon \rho^\gamma q_6(x)) \\ Q_7(x, \rho) &= \Omega_\psi (1 + \epsilon \rho^\gamma q_7(x)) \\ Q_8(x, \rho) &= Q_{\text{NH}} (1 + \epsilon \rho^\gamma q_8(x)) \\ Q_9(x, \rho) &= \beta(x) (1 + \epsilon \rho^\gamma q_9(x)) \\ Q_{10}(x, \rho) &= \delta(x) (1 + \epsilon \rho^\gamma q_{10}(x)) , \end{aligned} \quad (4.2)$$

with ϵ a bookkeeping parameter that we take to be infinitesimally small. (Note that this is different from the expansion parameter ε we used to add angular momenta.) When $\epsilon = 0$ we get Eq. (3.6), showing that we are perturbing the appropriate near-horizon geometry. For any $\gamma \neq 0, 1$ the Einstein equation implies that

$$q_2(x) = q_3(x) + q_4(x) . \quad (4.3)$$

For exactly $\gamma = 0, 1$ we still impose the above, but as a gauge condition instead, which can be achieved via a residual gauge symmetry similar to the one found in [6]. The resulting perturbed Einstein and Maxwell equations yield first order differential equations for q_1 and q_3 and seven second order equations for the remaining variables. These are the equations that one wishes to solve in perturbation theory about $\varepsilon \ll 1$, i.e. small angular momenta. Note that Γ , σ_I , α , β , δ and A_I admit themselves an expansion in terms of ε (see Eqs. (3.10)), and we would like to determine γ using said expansion.

Let $q_i^{(0)}(x)$ and $\gamma^{(0)}$ denote a solution to these equations with $\varepsilon = 0$, that is before we add angular momenta. So $\gamma^{(0)}$ is a scaling dimension of the static $U(1) \times U(1)$ symmetric near-horizon geometry found in [8]. With $\varepsilon = 0$, the equations decouple into three groups:

$$G_1 \equiv \left\{ q_1^{(0)}, q_3^{(0)}, q_4^{(0)}, q_8^{(0)} \right\} , \quad G_2 \equiv \left\{ q_5^{(0)} \right\} , \quad \text{and} \quad G_3 \equiv \left\{ q_6^{(0)}, q_7^{(0)}, q_9^{(0)}, q_{10}^{(0)} \right\} . \quad (4.4)$$

We first study the modes with the lowest scaling dimension since they will dominate near the horizon. This turns out to be $\gamma^{(0)} = 0$. Using this fact and imposing regularity at $x = 0$ and $x = 1$ we find⁵

$$\begin{aligned}
q_1^{(0)}(x) &= q_2^{(0)}(x) = \left[\frac{2c_1c_2}{\sigma(x)} - c_1 - c_2 \right] a_0, & q_3^{(0)}(x) &= \left[\frac{c_1c_2}{\sigma(x)} - 2c_1 + c_2 \right] a_0, \\
q_4^{(0)}(x) &= \left[\frac{c_1c_2}{\sigma(x)} - 2c_2 + c_1 \right] a_0, & q_5^{(0)}(x) &= a_2 + a_3 + \left[\frac{c_1c_2}{\sigma(x)} - 2c_1 + c_2 \right] a_0, \\
q_6^{(0)}(x) &= a_2, & q_7^{(0)}(x) &= a_3, & q_8^{(0)}(x) &= a_1 + (1 - 2x^2)(c_1 - c_2) \frac{a_0}{2}, \\
q_9^{(0)}(x) &= \frac{1}{1 + 2\lambda} \left\{ a_2 + 2a_3\lambda - \left[\frac{c_1c_2}{\sigma(x)} - 2c_1 + (1 - 2\lambda)c_2 \right] a_0 \right\}, \\
q_{10}^{(0)}(x) &= \frac{1}{1 + 2\lambda} \left\{ a_3 + 2a_2\lambda - \left[\frac{c_1c_2}{\sigma(x)} - 2c_2 + (1 - 2\lambda)c_1 \right] a_0 \right\}.
\end{aligned} \tag{4.5}$$

The solution depends on four undetermined parameters, a_0 , a_1 , a_2 , and a_3 , so there is a 4-fold degeneracy of modes with $\gamma^{(0)} = 0$. To see how γ changes when we add angular momenta, we use degenerate perturbation theory in ε .

We set the perturbation theory in ε as follows:

$$q_I(x) = \sum_{i=0}^{+\infty} \varepsilon^i q_I^{(i)}(x) \quad \text{with} \quad I = 1, \dots, 10 \quad \text{and} \quad \gamma = \sum_{i=1}^{+\infty} \varepsilon^i \gamma^{(i)}, \tag{4.6}$$

with all the $q_I^{(0)}(x)$ given above. To order ε , we find no constraints on a_0 , a_1 , a_2 and a_3 , but we find that $\gamma^{(1)} = 0$. This implies that γ does not change sign when we change the sign of J_i .

The equations at quadratic order become more complicated to solve, but nevertheless can be integrated in full generality. In particular, we can still decouple the $q_I^{(2)}$ according to the same groups as in Eq. (4.4), with the upperscript $^{(0)}$ replaced by $^{(2)}$. After some lengthy algebra we find that the smallest scaling dimension becomes

$$\gamma = 2\sqrt{3}\pi \frac{1 - \lambda^2}{4 - \lambda^2} \frac{J_\phi J_\psi}{Q^3} + \mathcal{O}(\varepsilon^3). \tag{4.7}$$

and that the relation between a_0 , a_1 , a_2 , and a_3 becomes determined, in accordance to general expectations from degenerate perturbation theory. We have assumed that the angular momenta and charge are positive. If not, the J_i 's and Q should be replaced by their absolute value, so γ is positive for $|\lambda| < 1$. The fact that γ becomes negative for $|\lambda| > 1$ strongly suggests that the near-horizon geometries will cease to smoothly connect to an asymptotically flat end when $|\lambda| > 1$.

We now discuss some of the modes of the zeroth order static geometries with larger scaling dimensions. Although they are subdominant at small angular momenta, we will see

⁵Throughout these intermediate calculations we are assuming that 2λ is not an integer. However, our final result can be analytically continued to these semi-integer values.

that without the Chern-Simons term ($\lambda = 0$), there is “level crossing” as one increases J_i , and these modes can have smaller scaling dimension than the one starting at $\gamma^{(0)} = 0$. Recall that when $\varepsilon = 0$, the linearized equations decouple into three groups (4.4). The corresponding scaling dimensions for G_1 and G_2 can be determined analytically for any values of the squashing parameters c_1 and c_2 in Eq. (3.5), and they are found to be integers. The details of this calculation can be found in appendix A. However, for G_3 , we were only able to determine the scaling dimensions analytically in the special case $c_1 = c_2$, which corresponds to the near-horizon geometry of an extremal 5D Reissner-Nordström black hole. For $c_1 \neq c_2$ we will proceed numerically.

When $c_1 = c_2$, we can exploit the background spherical symmetry to decompose the functions in G_3 using vector spherical harmonics on S^3 . This reduces the task of determining the scaling dimensions to solving an algebraic problem. Within our symmetry class, vector spherical harmonics on S^3 are simply given by

$$S_{\hat{a}}^{\phi} dx^{\hat{a}} = \frac{S(x)}{1-x^2} d\phi \quad \text{and} \quad S_{\hat{a}}^{\psi} dx^{\hat{a}} = \frac{S'(x)}{x} d\psi \quad (4.8)$$

where $\hat{a} = \{x, \phi, \psi\}$ and

$$S(x) = {}_2F_1(-p-1, p+1; 1; x^2) \quad (4.9)$$

with $p = 0, 1, 2 \dots$ and ${}_2F_1(a, b; c; z)$ the standard Gauss hypergeometric function. Using the above, we set

$$q_6^{(0)}(x) = \frac{S(x)}{1-x^2} a_0, \quad q_7^{(0)}(x) = \frac{S'(x)}{x} b_0, \quad q_9^{(0)}(x) = \frac{S(x)}{1-x^2} c_0 \quad \text{and} \quad q_{10}^{(0)}(x) = \frac{S'(x)}{x} d_0 \quad (4.10)$$

where a_0, b_0, c_0 and d_0 are constants to be determined. Plugging in the above into the G_3 equations with $c_1 = c_2$, yields an eigenvalue equation for γ , with the a_0, b_0, c_0 and d_0 regarded as the components of an eigenvector. Once the dust settles, we find four families of modes. Modes with $p = 0$ are special, so we discuss these first.

When $p = 0$ the four families of modes are given by

$$\gamma^{(0)} = 0, \quad \gamma_{\pm}^{(0)} = \frac{1}{2} \left(\sqrt{17 \pm 8\lambda} - 1 \right) \quad (4.11)$$

where the mode with $\gamma^{(0)} = 0$ has degeneracy two⁶, i.e. one can express c_0 and d_0 as a function of *both* a_0 and b_0 . This special mode persists even when $c_1 \neq c_2$ and was discussed above. Note that one can map γ_+ into γ_- by flipping the sign of λ , so we take $\lambda > 0$ without loss of generality. γ_+ is positive and real for all values of $\lambda > 0$, however, γ_- exhibits a more interesting behaviour. Namely, it becomes negative for $\lambda > 2$, and complex for $\lambda > 17/8$. A negative γ signals a breakdown of perturbation theory and indicates that the full asymptotically flat solution does not approach the near-horizon geometry. A complex

⁶We showed above that $\gamma^{(0)} = 0$ has four-fold degeneracy, but here we are only considering the equations in group G_3 which correspond mainly to perturbations of the Maxwell field.

γ means that the mode has an effective AdS_2 mass below the 2D Breitenlohner-Friedman bound. This implies that there is a dynamical instability of the near extremal asymptotically flat black hole when $\lambda > 17/8$ [23].

For $p \geq 1$ we find the following four families of modes (dropping the 0 superscript)

$$\gamma_{\pm}^+ = \sqrt{\frac{1}{4} + [2 + \lambda(p+1)] + p(p+2)} \pm \sqrt{[2 + \lambda(p+1)]^2 + 3p(p+2)} - \frac{1}{2}. \quad (4.12a)$$

and

$$\gamma_{\pm}^- = \sqrt{\frac{1}{4} + [2 - \lambda(p+1)] + p(p+2)} \pm \sqrt{[2 - \lambda(p+1)]^2 + 3p(p+2)} - \frac{1}{2}. \quad (4.12b)$$

Since we can map the γ_{\pm}^- modes to the γ_{\pm}^+ modes by flipping the sign of λ , we will again take $\lambda > 0$ without loss of generality. The γ_{\pm}^+ , γ_{+}^- modes are always real and positive, but γ_{-}^- becomes negative when $\lambda > (1+p)/2$. In fact, for $p = 1$, this happens precisely when $\lambda > 1$, suggesting that the region $\lambda > 1$ does not admit a smooth zero temperature limit if modes with $p \geq 1$ are excited in the near-horizon region. What is more, if we increase λ further, we find that γ_{-}^- becomes complex for

$$\lambda > \frac{16p^4 + 64p^3 + 88p^2 + 48p + 17}{32p^3 + 96p^2 + 72p + 8} \quad (4.13)$$

signaling a dynamical instability of the full extremal geometry for any value of p .

To calculate these scaling dimensions for the nonspherical near-horizon geometries, we proceed numerically. All physical results depend only on the ratio of the squashing parameters $c_2/c_1 \equiv \alpha$. Furthermore, since sending α to $1/\alpha$ merely exchanges $x = 0$ with $x = 1$, which is an isometry that relabels ϕ as ψ and vice versa, we can restrict α to the range $0 < \alpha < 1$.

To proceed we define

$$q_6^{(0)}(x) = \gamma r_1(x), \quad q_7^{(0)}(x) = \gamma r_2(x), \quad q_9^{(0)}(x) = \sqrt{c_1 c_2} r_3(x) \quad \text{and} \quad q_{10}^{(0)}(x) = \sqrt{c_1 c_2} r_4(x) \quad (4.14)$$

and solve for $\{r_i, \gamma(\gamma+1)\}$ numerically as a function of α and λ . Note that since we are solving for $\gamma(\gamma+1)$, γ will become complex if $\gamma(\gamma+1) < -1/4$. When $\alpha = 1$, we recover the analytic results discussed above. At $x = 1$ we impose regularity, which yields Robin-type boundary conditions for all eigenfunctions r_i , and similarly at $x = 0$. The resulting second order equations are solved numerically using a spectral collocation grid in the x direction, on Gauss-Lobatto nodes.

In Fig. 3, we plot $\gamma(\gamma+1)$ as a function of λ for several fixed values of α , indicated on the right. We focused on extending the modes γ_{-}^- with $p = 1$ when $c_1 = c_2$ (blue disks in Fig. 3), as these impose the strongest constraints on the physical range of λ . The horizontal black dashed line represents $\gamma(\gamma+1) = -1/4$, and any points below this line correspond to complex values of γ . We see that this occurs for all α as we increase λ indicating that near extremal black holes become unstable [23].⁷ For $\lambda > 1$ all these scaling dimensions become negative,

⁷The fact that black holes can be unstable when $\lambda > 1$ was discussed in [24].

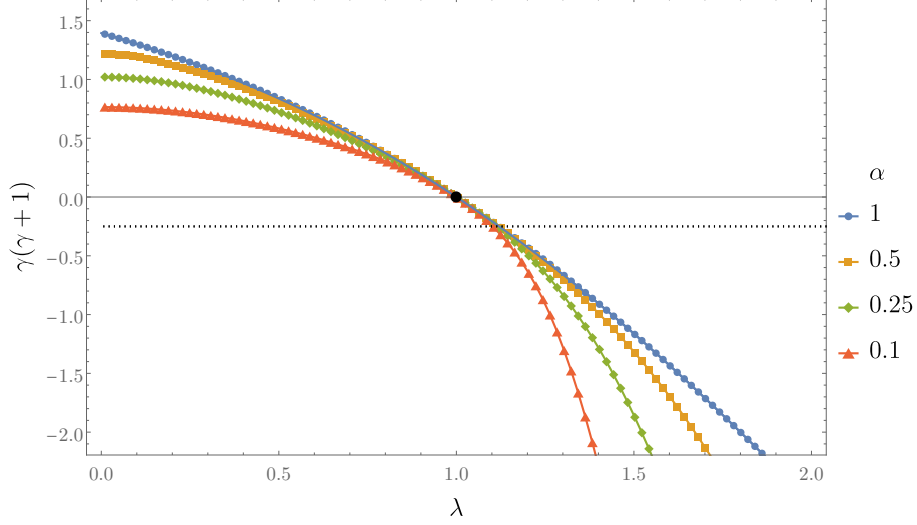


Figure 3. $\gamma(\gamma + 1)$ as a function of the Chern-Simons coefficient λ , for several fixed values of the squashing parameter $\alpha \equiv c_2/c_1$ (3.5), indicated on the right. Note that $\gamma < 0$ for $\lambda > 1$ indicating that the extremal black hole has a singular horizon with diverging curvature scalars. The horizontal black dashed line represents $\gamma(\gamma + 1) = -1/4$, and any points below this line will necessarily have complex values of γ indicating an instability of the near extremal black hole.

for any value of α , signaling that if modes with $p = 1$ are turned on in the near-horizon region, perturbation theory breaks down. We will show in section 5 that these modes are sourced just by adding an asymptotically flat region, with the result that curvature scalars now diverge on the horizon in the extremal limit.

4.2 Perturbative in the charge

In this section, we compute the scaling dimensions perturbatively in the charge. It is helpful to make a slight gauge adjustment to match the known form of the near-horizon geometry of an extremal Myers-Perry black hole. We now take the following metric and gauge field ansatz

$$ds^2 = Z_1(x, \rho) \left\{ -\rho^2 dT^2 + \frac{d\rho^2}{\rho^2} + \frac{Z_7(x, \rho) dx^2}{1 - x^2} + Z_2(x, \rho)(1 - x^2) (d\phi + \rho Z_5(x, \rho) dT)^2 \right. \\ \left. + Z_4(x, \rho)x^2 [d\psi + \rho Z_6(x, \rho) dT + (1 - x^2)Z_3(x, \rho) (d\phi + \rho Z_5(x, \rho) dT)]^2 \right\}, \quad (4.15a)$$

and

$$A = -Z_8(x, \rho) dT + Z_9(x, \rho)(1 - x^2) (d\phi + \rho Z_5(x, \rho) dT) + \\ Z_{10}(x, \rho)x^2 [d\psi + \rho Z_6(x, \rho) dT + (1 - x^2)h_{12}(x, \rho) (d\phi + \rho Z_5(x, \rho) dT)] , \quad (4.15b)$$

with a total of ten functions $Z_I(x, \rho)$ to solve for. Since we are interested in computing the scaling dimensions γ , we set

$$\begin{aligned}
Z_1(x, \rho) &= \Gamma(x) [1 + \epsilon \rho^\gamma z_1(x)] , \\
Z_2(x, \rho) &= h_{11}(x) [1 + \epsilon \rho^\gamma z_2(x)] , \\
Z_3(x, \rho) &= h_{12}(x) [1 + \epsilon \rho^\gamma z_3(x)] , \\
Z_4(x, \rho) &= h_{22}(x) [1 + \epsilon \rho^\gamma z_4(x)] , \\
Z_5(x, \rho) &= \Omega_\phi [1 + \epsilon \rho^\gamma z_5(x)] , \\
Z_6(x, \rho) &= \Omega_\psi [1 + \epsilon \rho^\gamma z_6(x)] , \\
Z_7(x, \rho) &= \Gamma_{\text{NH}} [1 + \epsilon \rho^\gamma z_7(x)] , \\
Z_8(x, \rho) &= Q_{\text{NH}} + \epsilon \rho^\gamma z_8(x) , \\
Z_9(x, \rho) &= b_1(x) [1 + \epsilon \rho^\gamma z_9(x)] , \\
Z_{10}(x, \rho) &= b_1(x) [1 + \epsilon \rho^\gamma z_{10}(x)] ,
\end{aligned} \tag{4.16}$$

where ϵ is a bookkeeping parameter assumed to be infinitesimally small. Linearising around $\epsilon = 0$, yields a linear set of equations coupling all ten functions z_I and the corresponding scaling dimension γ .

For $\gamma \neq 0, 1$, the Einstein equation implies that

$$z_7 = -\frac{3}{2}z_1 - \frac{1}{2}z_2 - \frac{1}{2}z_4 , \tag{4.17}$$

while for $\gamma = 0, 1$ we can impose the above relation as a gauge choice. The remaining equations yield two first order constraints on the z_I , and seven second order ordinary differential equations in total. The two first order constraints are then combined to give a second order differential equation. Once the dust settles, these can be combined into a set of eight second order differential equations for $z_1, z_2, z_4, z_5, z_6, z_8, z_9$ and z_{10} which are all coupled.

We solve these equations perturbatively in the black hole charge. Using the same expansion we used in Eqs. (3.20), we set

$$z_I(x) = \sum_{i=0}^{+\infty} q^i z_I^{(i)}(x) \quad \text{and} \quad \gamma = \sum_{i=0}^{+\infty} q^i \gamma^{(i)} , \tag{4.18}$$

so that at zeroth order in q , we are simply computing the scaling dimensions $\gamma^{(0)}$ of the near-horizon geometry of an extremal Myers-Perry black hole. These can be computed in full generality, as shown in Appendix B, and turn out to be nonnegative integers, consistent with earlier results in the literature [23, 25]. We are primarily interested in the lowest scaling dimension, which is $\gamma^{(0)} = 0$.

Even for $\gamma^{(0)} = 0$, the explicit expressions are somewhat cumbersome for several of the functions. However, to facilitate the reproduction of the calculations in this paper, we present

a few examples here, highlighting the main features:

$$\begin{aligned}
z_3^{(0)}(x) &= \frac{1}{x^2 + 4\Omega_\phi^2} \left[\mu_0 x^2 + 2\mu_1 \Omega_\phi^2 \left(4 - \frac{137 + 965\Omega_\phi^2 - 4745\Omega_\phi^4 + 3003\Omega_\phi^6}{1384 - 4337\Omega_\phi^2 - 4061\Omega_\phi^4 + 13809\Omega_\phi^6 + 3573\Omega_\phi^8} x^2 \right) \right] \\
z_5^{(0)}(x) &= -\mu_1, \\
z_6^{(0)}(x) &= \mu_1, \\
z_8^{(0)}(x) &= 0, \\
z_9^{(0)}(x) &= \frac{\nu_0 + 4\Omega_\phi^2 \nu_1}{x^2 + 4\Omega_\phi^2}, \\
z_{10}^{(0)}(x) &= \nu_1 + \frac{4\Omega_\phi^2 \nu_0}{x^2 + 4\Omega_\phi^2(1 - x^2)}.
\end{aligned} \tag{4.19}$$

where $\mu_0, \mu_1, \nu_0, \nu_1$ are arbitrary constants. The remaining functions not shown, i.e., $z_1^{(0)}(x)$, $z_2^{(0)}(x)$, $z_4^{(0)}(x)$, and $z_7^{(0)}(x)$, depend only on x , μ_0 , and μ_1 . The discussion above demonstrates that the near-horizon geometry of an extreme Myers-Perry black hole has a fourfold degeneracy for modes with vanishing scaling dimension. We then proceed to higher orders in q , applying degenerate perturbation theory. At first order in q , we find $\gamma^{(1)} = 0$, which is consistent with our expectation that the scaling dimensions should not depend on the sign of the electric charge. At first order, we also find that $\nu_0 = -\nu_1$, a constraint that ensures our deformations do not alter the background electric charge. At this stage, we find ourselves with a three-fold degeneracy which we can choose to parametrise by μ_0 , μ_1 and ν_1 .

The equations at second order become increasingly difficult to solve, but can still be solved in full generality. This is possible because the perturbations decouple into three groups at each i -th order in perturbation theory, and each group can be integrated separately. The groups in this case are:

$$G_1 = \{z_1^{(i)}, z_2^{(i)}, z_4^{(i)}\}, \quad G_2 = \{z_5^{(i)}, z_6^{(i)}\} \quad \text{and} \quad G_3 = \{z_8^{(i)}, z_9^{(i)}, z_{10}^{(i)}\}. \tag{4.20}$$

While this occurs for modes that smoothly connect to $\gamma^{(0)} = 0$ in the $q \rightarrow 0$ limit, in general, the functions in G_1 and G_2 mix for modes with $\gamma^{(0)} \neq 0$. At second order we finally determine $\gamma^{(2)}q^2$ after imposing regularity at $x = 0$ and $x = 1$. The expression appears as a function of a , Ω_ϕ and q , but we can readily rewrite these in terms of J_ϕ , J_ψ and Q , respectively. We find two possible solutions. Either $\gamma^{(2)}q^2 = 0$ and we need to proceed to fourth order to determine $\gamma^{(4)}q^4$ and the remaining degeneracy, or:

$$\begin{aligned}
\gamma &= \gamma_+^{(2)} q^2 + \mathcal{O}(q^3) \\
&= \frac{16^{1/3}}{3\pi^{2/3}} \frac{1}{J_\phi J_\psi} \frac{J_+^{2/3}}{J_-^2} \left[J_\phi^2 - 6J_\phi J_\psi + J_\psi^2 + 2J_\phi J_\psi \frac{J_+}{J_-} \log \left(\frac{J_\phi}{J_\psi} \right) \right] (1 - \lambda^2) Q^2 + \mathcal{O}(Q^3),
\end{aligned} \tag{4.21}$$

with $J_\pm \equiv J_\phi \pm J_\psi$. If we fix $J_\psi = \beta J_\phi$ with $\beta > 0$, the above expression predicts $\gamma \sim (|Q|^{3/2}/J_\phi)^{4/3}$ for large values of $J_\phi/|Q|^{3/2}$. This shows that the addition of charge indeed

lifts γ to a noninteger value causing the horizon to become singular. Notice that at least for small values of $|Q|^{3/2}/J_\phi$, where we expect perturbation theory to be valid, $\gamma < 0$ for $\lambda > 1$. This indicates that we do not expect these particular near-horizon geometries to smoothly connect to an asymptotically flat region.

Even though there appears to be a divergence in (4.21) when $J_\phi = J_\psi$, this is not the case. Indeed, in the limit $J_\phi \rightarrow J_\psi$ the above expression collapses to

$$\gamma = \frac{16}{9\pi^{2/3}} (1 - \lambda^2) \frac{Q^2}{J_\psi^{4/3}} + \mathcal{O}(Q^3). \quad (4.22)$$

4.3 Fully nonlinear results

In this section, we avoid approximations and solve for the scaling dimensions γ numerically. Since we want to use the backgrounds constructed in section 3.3, we again use the De Turck trick. Our metric and gauge field ansatz read

$$\begin{aligned} ds^2 = & -\rho^2 Q_1(x, \rho) dT^2 + \frac{Q_8(x, \rho) (d\rho + \rho Q_9(x, \rho) dx)^2}{\rho^2} \\ & + 4 \left\{ \frac{Q_2(x, \rho) dx}{1 - x^2} + (1 - x^2) Q_3(x, \rho) (d\phi + \omega_\phi \rho Q_{10}(x, \rho) dT)^2 \right. \\ & \left. + x^2 Q_4(x, \rho) [d\psi + \omega_\psi \rho Q_{11}(x, \rho) dT + (1 - x^2) Q_5(x, \rho) (d\phi + \omega_\phi \rho Q_{10}(x, \rho) dT)]^2 \right\}, \end{aligned} \quad (4.23a)$$

$$\begin{aligned} A = & -Q_{\text{NH}} \rho Q_{12}(x, \rho) + (1 - x^2) Q_6(x, \rho) (d\phi + \omega_\phi \rho Q_{10}(x, \rho) dT) + \\ & x^2 Q_7(x, \rho) [d\psi + \omega_\psi \rho Q_{11}(x, \rho) dT + (1 - x^2) Q_5(x, \rho) (d\phi + \omega_\phi \rho Q_{10}(x, \rho) dT)] , \end{aligned} \quad (4.23b)$$

with a total of twelve functions $Q_I(x, \rho)$ to solve for. For our reference metric, we take

$$\begin{aligned} Q_1(x, \rho) = Q_2(x, \rho) = Q_3(x, \rho) = Q_4(x, \rho) = Q_8(x, \rho) = Q_{10}(x, \rho) = Q_{11}(x, \rho) = 1, \\ Q_5(x, \rho) = Q_9(x, \rho) = 0, \end{aligned} \quad (4.24)$$

which was precisely the reference metric used in section 3.3. To proceed, we define

$$\begin{aligned} Q_I(x, \rho) &= Q_I(x) [1 + \epsilon \rho^\gamma q_I(x)] , \quad \text{for } I = 1, \dots, 7 \\ Q_8(x, \rho) &= Q_1(x) [1 + \epsilon \rho^\gamma q_8(x)] , \\ Q_9(x, \rho) &= \epsilon \rho^\gamma q_9(x) , \\ Q_I(x, \rho) &= 1 + \epsilon \rho^\gamma q_I(x) \quad \text{for } I = 10, 11, 12. \end{aligned} \quad (4.25)$$

As expected, the dependence on ρ cancels out, leaving us with twelve ordinary differential equations of the Sturm-Liouville type for the $q_I(x)$, with γ appearing as an eigenvalue.

The boundary conditions at $x = 0$ and $x = 1$ are determined by regularity. At $x = 0$, Neumann boundary conditions apply to all variables except for q_9 , which satisfies a Dirichlet condition, $q_9(0) = 0$. Additionally, there is a Dirichlet condition that imposes $q_2(0) = q_4(0)$. For $x = 1$, we apply Robin-type boundary conditions to all variables, along with a Dirichlet condition $q_2(1) = q_3(1)$.

The resulting Sturm-Liouville problem is solved using spectral collocation methods, discretized on a Gauss-Lobatto grid with N collocation points. As expected, we observe exponential convergence as N increases, which is characteristic of spectral collocation methods. Additionally, we monitor $\xi_a \xi^a$ and find that it approaches zero in the continuum limit, i.e., as N increases, with exponential speed. All the plots presented in this section were generated with $N = 200$.

In Fig. 4 we plot the scaling dimension amenable to the perturbative analysis discussed in Sections 4.1 and 4.2 as a function of the normalised angular momentum $J_\phi/|Q|^{3/2}$. This figure was generated for fixed values of $\lambda = 0$ and $J_\psi = 3J_\phi/8$. We also plot the perturbative calculation valid at small angular momenta given in Eq. (4.7) (black dotted line) and the perturbative prediction valid at small charge and given in Eq. (4.21) (black dashed line). In both cases, the agreement is excellent. The same color coding as in Fig. 1 is used. The family of near-horizon geometries represented in orange in Fig. 1 is observed to have negative scaling dimensions, supporting the earlier claim that it cannot be connected to an asymptotically flat end. The family of near-horizon geometries represented in blue in Fig. 1 always has small *positive* scaling dimensions, with $0 < \gamma < 1/2$. Although we have chosen $J_\psi/J_\phi = 3/8$, we have observed this to be the case for a large range of values of J_ψ/J_ϕ .

In Fig. 5 we show the two smallest values of the scaling dimension γ as a function of the normalised angular momentum $J_\phi/|Q|^{3/2}$ using the same choice of parameters as in Fig. 4. When $J_\phi = 0$, we see two modes that are of interest. One of the modes starts at $\gamma = 0$ and was identified in Section 4.2. The second mode, with $\gamma \approx 0.733667(4)$ when $J_\phi = 0$, belongs to the G_3 -type eigenvalues identified in the same section, calculated for the squashed near-horizon geometry with $c_2/c_1 = \sqrt{3/8}$. This latter identification follows from Eq. (3.14). This figure also shows that for sufficiently large values of $J_\phi/|Q|^{3/2}$ the mode that dominates (with lowest scaling dimension) is not the one that dominates for small values of $J_\phi/|Q|^{3/2}$. Indeed, we can read off the scaling of γ at large $J_\phi/|Q|^{3/2}$ and, at finite $J_\phi/|Q|^{3/2}$, it appears to be consistent with $(|Q|^{3/2}/J_\phi)^{8/3}$, suggesting that this term can only be found by performing perturbation theory up to order q^4 about the near-horizon geometry of an extremal Myers-Perry black hole. This is consistent with the analysis of section 4.2.

We now briefly discuss the $\lambda \neq 0$ case. For $\lambda = 1$, all the scaling dimensions become integers. This is to be expected, since a known solution exists and is analytic in ρ when changed to the relevant gauge (see Eq. (3.3) for the corresponding near-horizon geometry). For $\lambda > 1$ we always find negative scaling dimensions for at least one mode. These connect to the modes generated by G_3 discussed in section 4.1. For $0 < \lambda < 1$ more interesting dynamics takes place. In particular, the orange and green families displayed in Fig. 2 both

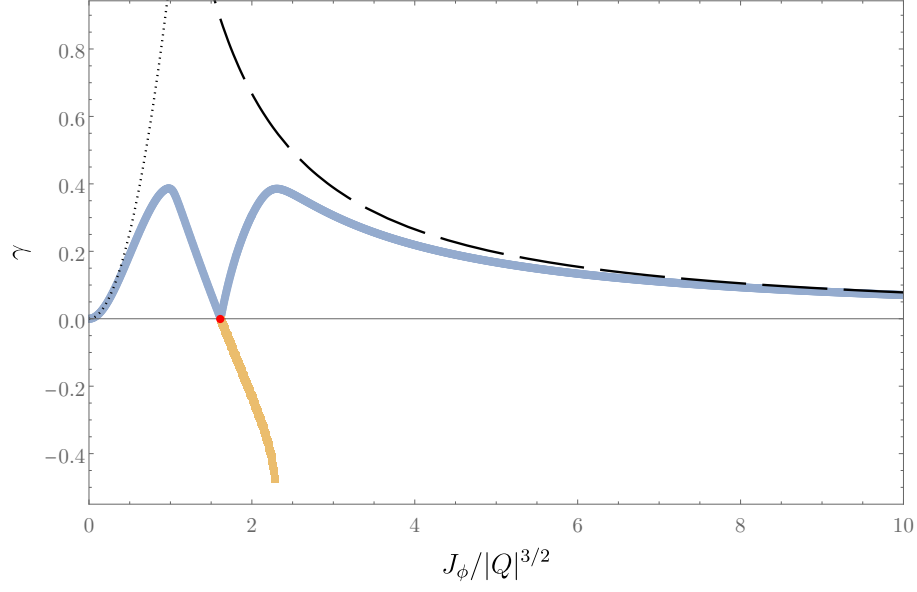


Figure 4. The scaling dimension of a mode on the general near-horizon geometry, as a function of the dimensionless angular momentum $J_\phi/|Q|^{3/2}$. The same color coding as in Fig. 1 is used. The perturbative calculation, valid at small angular momenta and given in Eq. (4.7) (black dotted line), as well as the perturbative prediction valid at small charge, provided in Eq. (4.21) (black dashed line), are shown. This figure was generated for fixed values of $\lambda = 0$ and $J_\psi = 3J_\phi/8$.

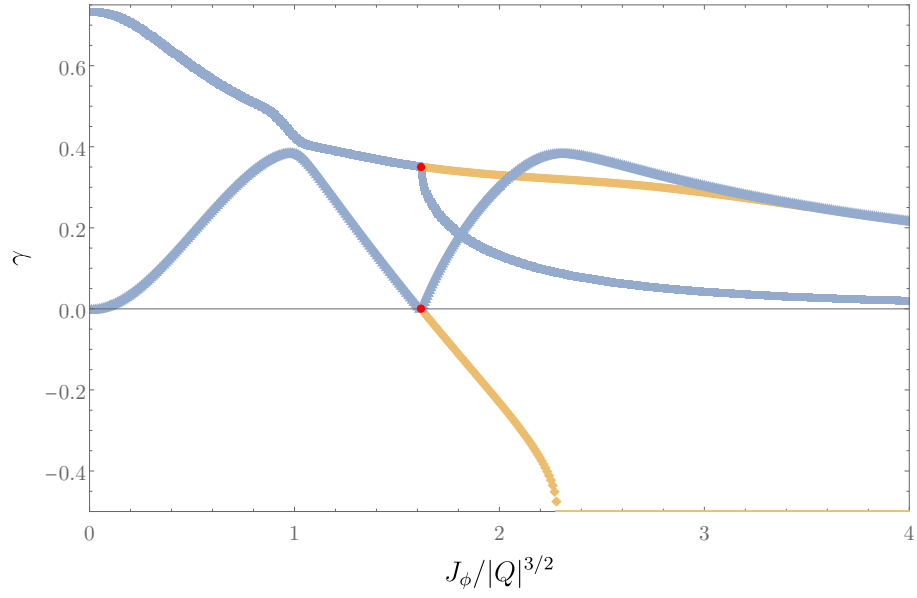


Figure 5. The two lowest scaling dimensions γ that we found numerically as a function of the dimensionless angular momentum $J_\phi/|Q|^{3/2}$, for fixed values of $\lambda = 0$ and $J_\psi = 3J_\phi/8$. Notice that the mode with smallest γ changes as we increase $J_\phi/|Q|^{3/2}$.

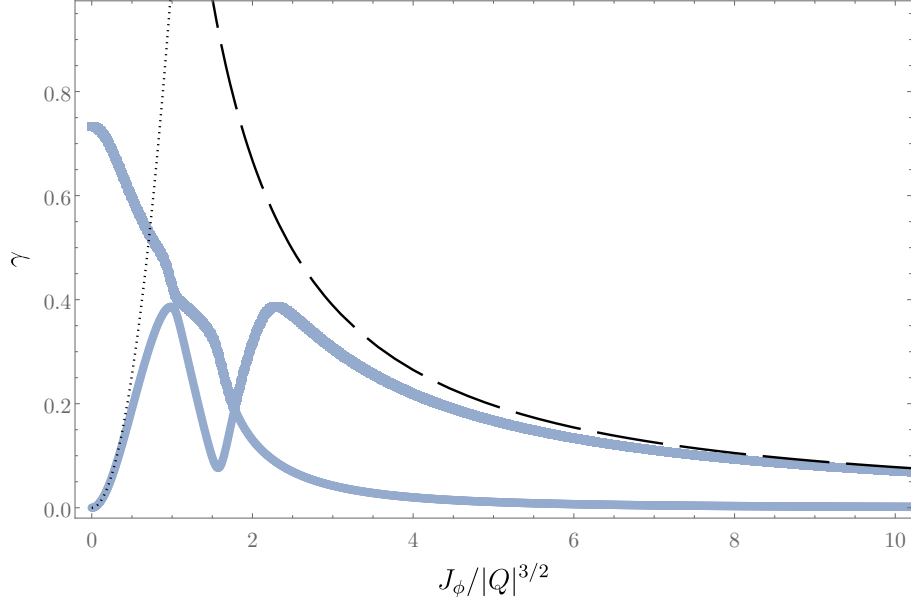


Figure 6. The two lowest scaling dimensions γ that we found numerically as a function of dimensionless angular momentum $J_\phi/|Q|^{3/2}$ for fixed values of $\lambda = 10^{-2}$ and $J_\psi = 3J_\phi/8$.

have negative or complex scaling dimensions, showing that these are not suitable to connect to an asymptotically flat end.

Perhaps more interestingly, when $\lambda \neq 0$, the non-analytic behaviour observed in Fig. 4 and Fig. 5 is smoothed out. This is most clearly seen in Fig. 6, where we plot the two lowest-lying scaling dimensions as a function of the normalised angular momentum $J_\phi/|Q|^{3/2}$, for fixed $\lambda = 10^{-2}$ and $J_\psi = 3J_\phi/8$. The colour coding is similar to that used in Fig. 4; in particular, the perturbative calculation valid at small angular momenta (Eq. (4.7)) is shown by the black dotted line, while the perturbative prediction valid at small charge (Eq. (4.21)) is represented by the black dashed line.

Another interesting phenomenon that occurs at finite λ is level repulsion⁸. Specifically, the two branches of scaling dimensions that cross in Fig. 5 around $J_\phi/|Q|^{3/2} \approx 1.80273(5)$ split apart and open a gap for any $\lambda \neq 1$. This is difficult to visualize in Fig. 6 since $\lambda = 10^{-2}$. However, in Fig. 7, we plot the two lowest scaling dimensions for fixed $\lambda = 0.1$ and $J_\psi = 3J_\phi/8$, where this phenomenon can be clearly observed. So if the Chern-Simons term is included, the mode with lowest scaling dimension does not change as we increase the angular momentum.

⁸The phenomenon of eigenvalue repulsion in the context of black holes was first observed while studying the quasinormal modes of Kerr-Newman black holes in [26–31].

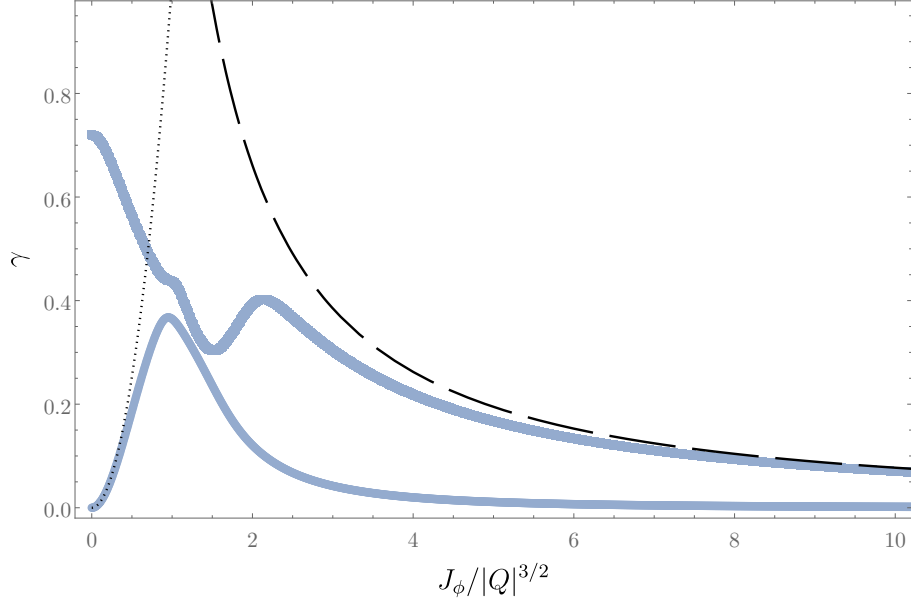


Figure 7. The two lowest scaling dimensions γ that we found numerically as a function of dimensionless angular momentum $J_\phi/|Q|^{3/2}$ for fixed values of $\lambda = 0.1$ and $J_\psi = 3J_\phi/8$. It is now clear that while the perturbative expressions (4.7) and (4.21) are accurate approximations to the exact result in their respective domains, they apply to different modes.

5 Near extremal black holes

We now shift focus slightly and proceed to numerically construct the domain of outer communications of near-extremal, electrically charged and rotating black hole solutions in Einstein-Maxwell-Chern-Simons theory. The aim of this section is to demonstrate that modes with non-integer scaling dimensions are generically present in the near-horizon region of rotating near-extremal black holes in this theory for any $\lambda \neq 1$. This includes the Einstein-Maxwell case (where $\lambda = 0$) and likely explains why electrically charged and rotating black holes in Einstein-Maxwell theory are not known in closed form. These non-integer scaling dimensions are responsible for both divergent tidal forces measured by the Weyl tensor and divergent electric fields.

5.1 Numerical method

To construct these solutions we use the same strategy as in [6], but adapted to five-dimensions. The idea is to use conformal coordinates, in which case the line element and gauge field ansatz reads

$$\begin{aligned}
 ds^2 = & -y^2 Q_1(x, y) \Delta(y) dt^2 + \frac{Q_2(x, y)}{1 - y^2} \left[\frac{dy^2}{(1 - y^2) \Delta(y)} + \frac{4dx^2}{2 - x^2} \right] \\
 & + \frac{1}{1 - y^2} \left[(1 - x^2)^2 Q_3(x, y) E_\phi^2 + x^2 (2 - x^2) Q_5(x, y) E_\psi^2 \right] \quad (5.1a)
 \end{aligned}$$

and

$$A = Q_8(x, y)(1 - y^2)dt + Q_9(x, y)(1 - x^2)^2 E_\phi + Q_{10}(x, y)x^2(2 - x^2)E_\psi, \quad (5.1b)$$

with

$$\begin{aligned} E_\phi &\equiv d\phi - (1 - y^2)^2 Q_4(x, y)dt, \\ E_\psi &= d\psi - (1 - y^2)^2 Q_6(x, y)dt + (1 - x^2)^2 Q_7(x, y)E_\phi, \\ \Delta(y) &= 1 - \frac{\tilde{Q}^2}{3}(1 - y^2)^2. \end{aligned} \quad (5.1c)$$

In the above, $(x, y) \in [0, 1]^2$, $\phi \sim \phi + 2\pi$, $\psi \sim \psi + 2\pi$, and $t \in \mathbb{R}$.

There are a total of ten functions Q_I of x and y to solve for. When $Q_1 = Q_2 = Q_3 = Q_5 = 1$, $Q_8 = \tilde{Q}$, $Q_4 = Q_6 = Q_7 = Q_9 = Q_{10} = 0$ we recover the line element of an electrically charged Reissner-Nordström black hole with the electric charge $\pi\tilde{Q}/(4)$. For this particular case, the map between standard spherical polar coordinates and the (x, y) coordinates reads

$$r = \frac{1}{1 - y^2} \quad \text{and} \quad x\sqrt{2 - x^2} = \cos\theta, \quad (5.2)$$

where we used the rescaling symmetry $g \rightarrow \hat{\lambda}^2 g$ and $A \rightarrow \hat{\lambda} A$ with $\hat{\lambda}$ constant to set the black hole event horizon radius to unity and $r \in (1, +\infty)$ and $\theta \in [0, \pi/2]$.

Spatial infinity is located at $y = 1$, where the round S^3 diverges in size and $g_{tt} \rightarrow -1$, while $x = 0$ and $x = 1$ correspond to the axes of symmetry generated by $\partial/\partial\phi$ and $\partial/\partial\psi$, respectively. The hypersurface $y = 0$ marks the location of the bifurcating Killing sphere. The Einstein equation demands that $Q_1(x, 0) = A_0$, $Q_2(x, 0) = w_\phi$, $Q_4(x, 0) = w_\psi$, $Q_6(x, 0) = w_\psi$ and $Q_8(x, y) = w_t$ with A_0 , w_ϕ , w_ψ and w_t being constant. Together, these statements imply that $y = 0$ is a Killing horizon generated by

$$K = \frac{\partial}{\partial t} + w_\phi \frac{\partial}{\partial \phi} + w_\psi \frac{\partial}{\partial \psi} \quad (5.3)$$

that is to say, $\|K\|^2 = 0$ at $y = 0$. The constants w_ϕ and w_ψ are interpreted as the angular velocities of the horizon, while w_t is the black hole chemical potential. The temperature can be computed via Eq. (2.6) and turns out to be given by

$$T = \frac{\sqrt{A_0}\Delta(0)}{2\pi} = \frac{\sqrt{A_0}}{2\pi} \left(1 - \frac{\tilde{Q}^2}{3} \right), \quad (5.4)$$

from which we conclude that as $\tilde{Q} \rightarrow \sqrt{3}^-$, $T \rightarrow 0^+$ as long as A_0 remains finite in the limit.

Following [6], we split the components of the Einstein equations into two sets: one that is solved directly on the grid, and another that is treated as constraints. Let

$$E_{ab} \equiv R_{ab} - \frac{1}{2}g_{ab}R - \frac{1}{2}\left(F_a{}^c F_{bc} - \frac{g_{ab}}{4}F^{cd}F_{cd}\right) \quad \text{and} \quad J^a \equiv \nabla_b F^{ba} - \frac{\lambda}{4\sqrt{3}}\epsilon^{abcde}F_{bc}F_{de} \quad (5.5)$$

We solve on the grid the following set of partial differential equations

$$\begin{aligned} D = \{E_{tt} = 0, g^{xx}E_{xx} + g^{yy}E_{yy} = 0, E_{t\phi} = 0, E_{t\psi} = 0, E_{\phi\phi} = 0, \\ E_{\phi\psi} = 0, E_{\psi\psi} = 0, J^t = 0, J^\phi = 0, J^\psi = 0\}. \end{aligned} \quad (5.6)$$

and for constraints we take

$$C_1 \equiv \frac{\sqrt{2-x^2}(1-y^2)\sqrt{\Delta}}{4}\sqrt{-g}(g^{xx}E_{xx} - g^{yy}E_{yy}) \quad \text{and} \quad C_2 \equiv (1-y^2)^2\Delta(y)\sqrt{-g}g^{xx}E_{xy}. \quad (5.7)$$

When all the equations in group D are satisfied, one can show that the constraints above obey

$$(1-y^2)\sqrt{\Delta(y)}\frac{\partial C_1}{\partial y} - 2\sqrt{2-x^2}\frac{\partial C_2}{\partial x} = 0, \quad (5.8a)$$

and

$$(1-y^2)\sqrt{\Delta(y)}\frac{\partial C_2}{\partial y} + 2\sqrt{2-x^2}\frac{\partial C_1}{\partial x} = 0. \quad (5.8b)$$

With a suitable choice of boundary conditions, detailed below, the two sets of equations above are sufficient to show that $C_1 = C_2 = 0$ throughout the integration domain if the equations in group D are satisfied. For additional details, we refer the reader to [6]. Furthermore, the equations in group D can be shown to be Elliptic, for the same choice of boundary conditions. This means that they can be readily solved using the numerical methods detailed in [21].

In order to understand the asymptotic structure at spatial infinity, we expand the equations of motion in a power series about $y = 1$. At each order in $(1-y)$, the equations decouple and can be readily solved after imposing regularity at $x = 0$ and $x = 1$. To the first order in $1-y$, we find:

$$\begin{aligned} Q_1(x, y) &= 1 + (1-y)\mathcal{E} + \mathcal{O}[(1-y)^2], \\ Q_2(x, y) &= 1 + (1-y) \left[\lambda_1 (2x^4 - 4x^2 + 1) - \frac{\mathcal{E}}{2} \right] + \mathcal{O}[(1-y)^2], \\ Q_3(x, y) &= 1 + \lambda_0(1-y) + \mathcal{O}[(1-y)^2], \\ Q_4(x, y) &= \mathcal{J}_\phi + (1-y) \left\{ \lambda_3 \left(x^4 - 2x^2 + \frac{1}{3} \right) + \frac{1}{3} [\mathcal{Q}\mu_\phi + 2\mathcal{J}_\phi (\mathcal{E} - \lambda_0)] \right\} + \mathcal{O}[(1-y)^2], \\ Q_5(x, y) &= 1 - (1-y) (\lambda_0 + \mathcal{E}) + \mathcal{O}[(1-y)^2], \\ Q_6(x, y) &= \mathcal{J}_\psi + (1-y) \left\{ \lambda_4 \left(x^4 - 2x^2 + \frac{2}{3} \right) + \frac{1}{3} [\mathcal{Q}\mu_\psi + 2\mathcal{J}_\psi (\lambda_0 + 2\mathcal{E})] \right\} + \mathcal{O}[(1-y)^2], \\ Q_7(x, y) &= \mathcal{O}[(1-y)^2] \\ Q_8(x, y) &= \mathcal{Q} + (1-y) \left[\lambda_5 \left(x^4 - 2x^2 + \frac{1}{2} \right) + \frac{\mathcal{Q}\mathcal{E}}{2} \right] + \mathcal{O}[(1-y)^2], \\ Q_9(x, y) &= (1-y)\mu_\phi + \mathcal{O}[(1-y)^2], \\ Q_{10}(x, y) &= (1-y)\mu_\psi + \mathcal{O}[(1-y)^2]. \end{aligned} \quad (5.9)$$

The constraints demand that

$$\lambda_0 + \lambda_1 + \frac{\mathcal{E}}{2} = 0 \quad (5.10)$$

which we regard as a Robin-type boundary condition for Q_2 , and thus impose at $y = 1$ that

$$\left(\frac{1}{2} \frac{\partial Q_1(x, y)}{\partial y} \Big|_{y=1} + \frac{\partial Q_5(x, y)}{\partial y} \Big|_{y=1} \right) (2 - 8x^2 + 4x^4) - \frac{\partial Q_1(x, y)}{\partial y} \Big|_{y=1} - 2 \frac{\partial Q_2(x, y)}{\partial y} \Big|_{y=1} = 0. \quad (5.11)$$

Using the asymptotic expansion above, we can readily compute the energy M , angular momenta (J_ϕ, J_ψ) and electric charge Q of these black hole solutions, which turn out to be given by

$$M = \frac{\pi}{16}(6 + 2\tilde{Q}^2 - 3\mathcal{E}), \quad J_\phi = \frac{\pi \mathcal{J}_\phi}{4}, \quad J_\psi = \frac{\pi \mathcal{J}_\psi}{4} \quad \text{and} \quad Q = \frac{\pi \mathcal{Q}}{4}. \quad (5.12)$$

As indicated above, at spatial infinity ($y = 1$), we impose that

$$Q_1(x, 1) = Q_3(x, 1) = Q_5(x, 1) = 1, \quad Q_4(x, 1) = \mathcal{J}_\phi, \quad Q_6(x, 1) = \mathcal{J}_\psi, \\ Q_8(x, 1) = \mathcal{Q} \quad \text{and} \quad Q_9(x, 1) = Q_{10}(x, 1) = 0, \quad (5.13)$$

together with Eq. (5.11). At the axis of symmetry generated by $\partial/\partial\psi$, i.e. $x = 0$, we demand that

$$\frac{\partial Q_I(x, y)}{\partial x} \Big|_{x=0} = 0, \quad \text{for } I = 1, \dots, 10 \quad (5.14)$$

together with $Q_2(0, y) = Q_5(0, y)$, with the latter condition ensuring that ψ has period 2π . Similarly, at $x = 1$, we demand that

$$\frac{\partial Q_I(x, y)}{\partial x} \Big|_{x=1} = 0, \quad \text{for } I = 1, \dots, 10 \quad (5.15)$$

together with $Q_2(1, y) = Q_3(1, y)$, thus ensuring that ϕ has period 2π .

Finally, we discuss the boundary conditions at the bifurcating Killing surface located at $y = 0$. The constraint equations impose constant temperature and constant angular velocity, but these are guaranteed to hold throughout the integration domain so long as the boundary conditions discussed above are imposed (see [6] for more details). As such, we impose Neumann boundary conditions on all variables at $y = 0$, i.e.

$$\frac{\partial Q_I(x, y)}{\partial y} \Big|_{y=0} = 0, \quad \text{for } I = 1, \dots, 10. \quad (5.16)$$

To recap, once we specify \tilde{Q} , \mathcal{Q} , \mathcal{J}_ϕ , and \mathcal{J}_ψ , we obtain a well-defined elliptic problem that can be readily solved using the methods detailed in [21]. Specifically, we discretize all the equations in group D in both the x and y directions using a spectral collocation approximation on two Gauss-Lobatto grids, with N_x and N_y points, respectively. The resulting discretised

equations are then solved using a standard Newton-Raphson routine. To check for convergence, we monitor the two constraints C_1 and C_2 , both of which approach zero exponentially fast as N_x and N_y increase, consistent with the expected convergence properties of spectral collocation methods. Note that up to factors of $\pi/(4)$, \mathcal{Q} , \mathcal{J}_ϕ , and \mathcal{J}_ψ directly control the electric charge and angular momenta, respectively. As such, our integration scheme allows us to cool down the black hole (by tuning \tilde{Q} close to $\sqrt{3}$) while keeping the electric charge and angular momenta constant.

5.2 Results

Without loss of generality, we will focus on solutions for which $J_\phi \geq J_\psi$. For such solutions, we expect the largest tidal forces to occur at $x = 0$. Rather than work with infalling timelike geodesics, we will study these effects using ingoing null geodesics. Thus, the first step is to consider affinely parameterised null geodesics $U^a = dx^a/d\lambda$, i.e., $U^a \nabla_a U^b = 0$ with $U^a U_a = 0$, which we now briefly discuss.

Our spacetime has three commuting Killing vector fields $\partial/\partial t$, $\partial/\partial \phi$ and $\partial/\partial \psi$. As such we expect three associated conserved charges. Let $\mathcal{L} = g_{ab} U^a U^b$, so that

$$E_n = -\frac{1}{2} \frac{\partial \mathcal{L}}{\partial \dot{t}}, \quad L_n^\phi = \frac{1}{2} \frac{\partial \mathcal{L}}{\partial \dot{\phi}} \quad \text{and} \quad L_n^\psi = \frac{1}{2} \frac{\partial \mathcal{L}}{\partial \dot{\psi}} \quad (5.17)$$

(where $\dot{\cdot} \equiv d/d\lambda$) are constants of motion. These conserved charges have no physical meaning (since they are not invariant under affine transformations), however, that is not the case for their ratio. Indeed, L_n^ϕ/E_n and L_n^ψ/E_n can be interpreted as the impact parameters of incoming geodesics. Using that all functions have Neumann boundary conditions at $x = 0$, it is a simple exercise to show null geodesics with $x(\lambda) = 0$ exist. We focus on geodesics along $x(\lambda) = 0$ with vanishing L_n^ϕ and L_n^ψ and using affine transformations we fix $E_n = 1$. From $g_{ab} U^a U^b = 0$ we can thus determine \dot{y} for such geodesics up to an overall sign. To fix the overall sign, we introduce Kerr-like ingoing coordinates in the vicinity of the future event horizon

$$\begin{aligned} dt &= dv - \frac{3}{2\sqrt{A_0}(3 - \tilde{Q}^2)} \frac{dY}{Y} \\ d\phi &= d\tilde{\phi} - \frac{3w_\phi}{2\sqrt{A_0}(3 - \tilde{Q}^2)} \frac{dY}{Y} + w_\phi dv \\ d\psi &= d\tilde{\psi} - \frac{3w_\psi}{2\sqrt{A_0}(3 - \tilde{Q}^2)} \frac{dY}{Y} + w_\psi dv. \end{aligned} \quad (5.18)$$

with $y = \sqrt{Y}$. Our black hole solutions are completely regular across $Y = 0$ in such coordinates, and since constant v hypersurfaces require $dY/dt < 0$, these coordinates are ingoing, and thus cover the future event horizon. It is in these coordinates that we want the ingoing geodesics to be regular, which in turn fixes the overall sign in \dot{y} . Once the dust settles we find that, in our original coordinates $\{t, x, y, \phi, \psi\}$,

$$U_a dx^a = -dt - \frac{\sqrt{Q_2(0, y)}}{y(1 - y^2)^{3/2} \sqrt{Q_1(0, y)} \Delta(y)} dy, \quad (5.19)$$

with our choice $E_n = 1$ also making U^a future-directed.

Tidal effects are traditionally measured using the Riemann tensor since this is the tensor that naturally enters the geodesic deviation equation. However, in the present context, the singularity is easier to measure using the following scalar quantity

$$\Phi = U^a \left(\frac{\partial}{\partial \phi} \right)^b F_{ab} \Big|_{x=0}. \quad (5.20)$$

This is analogous to the ϕ component of the electric field that an observer would measure along a timelike geodesic. If Φ diverges, the curvature cannot remain smooth. Since Φ is not invariant under rescalings $g \rightarrow \hat{\lambda}^2 g$ and $A \rightarrow \hat{\lambda} A$, with $\hat{\lambda}$ constant, we will always plot the rescaled quantity $\Phi \sqrt{|Q|}$, which is dimensionless.

We can also compute this quantity using our near-horizon analysis. Since the Maxwell field involves one derivative of the vector potential which is scaling like ρ^γ , one expects

$$\Phi \sqrt{|Q|} \propto \gamma \rho^{\gamma-1}, \quad (5.21)$$

and indeed, this is what we find. So any $0 < \gamma < 1$ will cause this quantity to diverge at the horizon of an extremal black hole.

For the remainder of this section, we will focus the case with $J_\psi/J_\phi = 3/8$, since this was used in previous sections. We have studied other linear combinations of angular momenta, and the qualitative results remain unchanged. We start by describing results in Einstein-Maxwell theory ($\lambda = 0$) and later show what happens for nonzero λ . In Fig. 8 we plot the rescaled entropy $S/|Q|^{3/2}$ as a function of the rescaled temperature $T\sqrt{|Q|}$ for fixed $J_\phi/|Q|^{3/2} = 8/(5\sqrt{\pi}) \approx 0.902703$. The black horizontal dashed line was obtained using the near-horizon geometries found in section 3.3. We see that as we cool down the black hole at fixed $J_\phi/|Q|^{3/2}$ and $J_\psi/|Q|^{3/2}$, the entropy precisely approaches that of the near-horizon geometries found in section 3.3. The agreement between the near-horizon analysis and full extremal black hole solution indicates that we have correctly identified the corresponding near-horizon geometry.

Not only can we match the entropy, but we can also match the local geometry of spatial cross-sections of the black hole event horizon. In Fig. 9, we present a parametric plot of $\{R_\phi, R_\psi\}/\sqrt{|Q|}$, where $R_\phi \equiv \sqrt{g_{\phi\phi}}$ and $R_\psi \equiv \sqrt{g_{\psi\psi}}$, along spatial cross-sections of the horizon. For a round three-sphere, this would result in a perfect quarter circle, but with rotation, the local geometry becomes deformed. The black dashed line is obtained using the near-horizon geometries found in 3.3, while the remaining curves are derived from the full black hole solution at different temperatures, labeled on the right. The agreement between these curves as the temperature decreases is further evidence that that we have correctly identified the relevant near-horizon geometry. This plot was generated with $\lambda = 0$ and $J_\psi/J_\phi = 3/8$, but we find a similar behaviour whenever the scaling dimensions found in section 4 are positive.

To see the singularity, we now turn our attention to the Maxwell field on the horizon. Given what we have seen before, one can expect Φ (defined in Eq. (5.20)) to become large as we

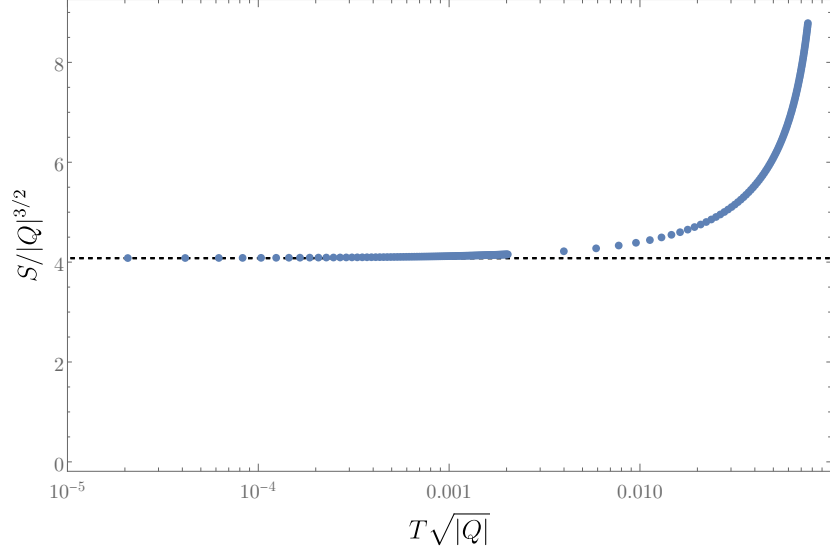


Figure 8. The rescaled entropy $S/|Q|^{3/2}$ as a function of the rescaled temperature $T\sqrt{|Q|}$ for fixed $J_\phi/|Q|^{3/2} = 8/(5\sqrt{\pi}) \approx 0.902703$, $J_\psi/J_\phi = 3/8$ and $\lambda = 0$. The black horizontal dashed lined was obtained using the near-horizon geometries found in section 3.3.

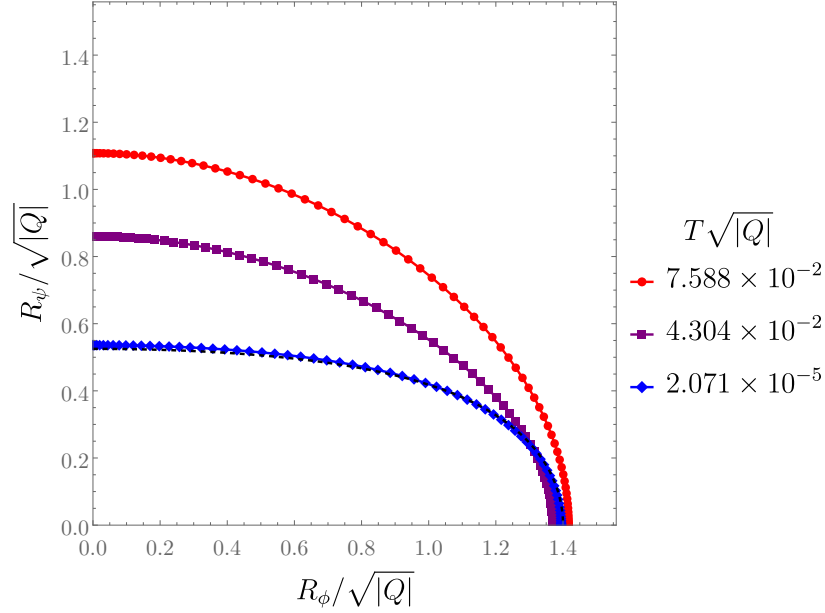


Figure 9. A parametric plot of $\{R_\phi, R_\psi\}/\sqrt{|Q|}$ along a spatial cross section of the black hole event horizon, with $R_\phi \equiv \sqrt{g_{\phi\phi}}$ and $R_\psi \equiv \sqrt{g_{\psi\psi}}$. The black dashed line corresponds to the near-horizon geometry found in section 3.3. All plots were generated with $J_\phi/|Q|^{3/2} = 8/(5\sqrt{\pi})$, $J_\psi/J_\phi = 3/8$, and $\lambda = 0$, and the different symbols correspond to the rescaled temperatures labelled on the right.

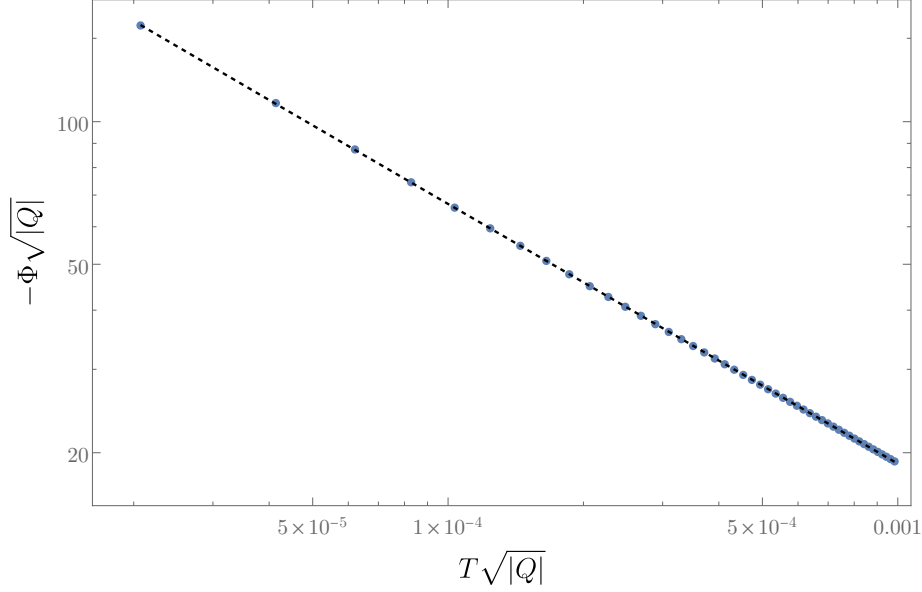


Figure 10. A log-log plot of $-\Phi\sqrt{|Q|}$ (defined in Eq. (5.20)) as a function of the rescaled temperature $T\sqrt{|Q|}$ for fixed $J_\phi/|Q|^{3/2} = 8/(5\sqrt{\pi})$, $J_\psi/J_\phi = 3/8$, and $\lambda = 0$. The black dashed line shows a fit to Eq. (5.22), with the predicted exponents computed in section 4.

lower the temperature. In Fig. 10 we plot $\Phi\sqrt{|Q|}$ as a function of the rescaled temperature, $T\sqrt{|Q|}$, in a log-log plot. This plot was again generated for $\lambda = 0$, $J_\psi/J_\phi = 3/8$ and $J_\phi/|Q|^{3/2} = 8/(5\sqrt{\pi})$. The divergence is very clearly seen across several decades. What is more, we can compare this divergence to the scaling dimensions found in the near-horizon analysis. Using the scaling argument in [7] one can relate the dependence on ρ of the extremal solution to the dependence on T for the near extremal solution. The net result is that we expect $\Phi\sqrt{|Q|} \sim \gamma T^{\gamma-1}$ where γ is the same scaling dimension computed in section 4. In fact we computed the two lowest scaling dimensions for these values of the parameters from the near-horizon analysis, and these turn out to be given by $\gamma_0 \approx 0.37709(5)$ and $\gamma_1 \approx 0.47806(9)$. The black dashed line shows a *two-parameter* fit to a curve of the form

$$f(\tau) \equiv a_0 \tau^{\gamma_0-1} + a_1 \tau^{\gamma_1-1} \quad (5.22)$$

for which we find $a_0 \approx 0.0614(5)$ and $a_1 \approx 0.3920(5)$. The agreement is excellent. In fact, the error in the fit is estimated to only affect the last digit of each of the constants reported above. If we try to fit with only one of the two terms, the fit is not accurate. Based on the above numbers, we can estimate when the first term dominates over the second. This happens for $T\sqrt{|Q|} \lesssim 10^{-8}$, which is outside what our numerical scheme can handle without resorting to extended precision and forbidden grid sizes.

Given this confirmation that the near-horizon analysis correctly describes the behavior of the full solution, it is clear that tidal forces will also diverge in the extremal limit:

$$R_{a\phi c\phi} U^a U^c \sim \gamma(\gamma-1) T^{\gamma-2}, \quad (5.23)$$

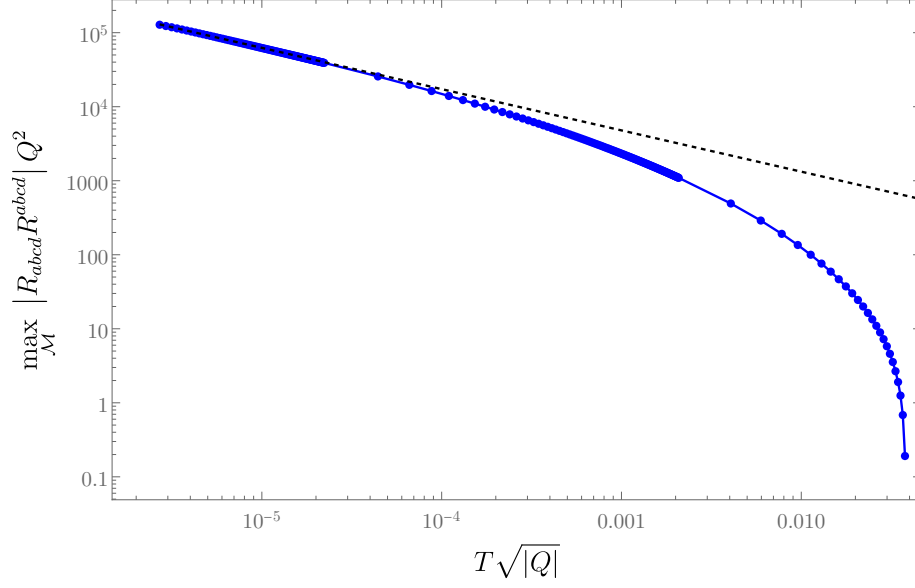


Figure 11. A log-log plot of the maximum of the absolute value of the normalised Kretschmann scalar $Q^2 R_{abcd} R^{abcd}$ as a function of the normalised temperature $T\sqrt{|Q|}$. This figure was generated for fixed $\lambda = 3/2$, $J_\psi/J_\phi = 3/8$ and $J_\phi/|Q|^{3/2} = 8/(5\sqrt{\pi})$. The black dashed line denotes the power law $T^{-0.557}$.

with R_{abcd} denoting the Riemann tensor.

When $|\lambda| > 1$, the situation becomes more intriguing. In this case, our near-horizon analysis consistently predicts the existence of at least one mode (possibly more) with a negative scaling dimension. This strongly suggests that smooth near-horizon geometries may not exist as we cool the black holes while keeping the electric charge and angular momenta constant. Indeed, in Fig. 11 we plot the maximum of the absolute value of the normalised Kretschmann scalar $Q^2 R_{abcd} R^{abcd}$ as a function of the normalised temperature $T\sqrt{|Q|}$. This figure was generated for fixed $\lambda = 3/2$, $J_\psi/J_\phi = 3/8$ and $J_\phi/|Q|^{3/2} = 8/(5\sqrt{\pi})$. The divergent curvature at small temperatures is consistent with an inverse power law scaling of the form $\max_{\mathcal{M}} |R_{abcd} R^{abcd}| Q^2 \propto T^{-0.557}$ (shown as a black dashed curve in Fig. 11).

The local geometry of spatial cross sections of the horizon also develops interesting features. In Fig. 12 we plot the normalised Ricci scalar of the spatial cross sections of the horizon, i.e. $\mathcal{R}|Q|$, as a function of the normalised proper distance from the ψ axis ($x = 0$), $\mathcal{P}/\sqrt{|Q|}$, with

$$\mathcal{P}(x) \equiv \int_0^x \frac{2\sqrt{Q_2(\tilde{x}, 0)}}{\sqrt{2 - \tilde{x}^2}} d\tilde{x}. \quad (5.24)$$

This figure was again generated at fixed $\lambda = 3/2$, $J_\psi/J_\phi = 3/8$ and $J_\phi/|Q|^{3/2} = 8/(5\sqrt{\pi})$. Fig. 12 shows that the Ricci scalar becomes very large, possibly diverging in the strict $T \rightarrow 0$ limit, as we lower the normalised temperature $T\sqrt{|Q|}$ at the axis of rotation generated by orbits of $\partial/\partial\psi$. This turns out to be the case whenever $J_\phi > J_\psi$.

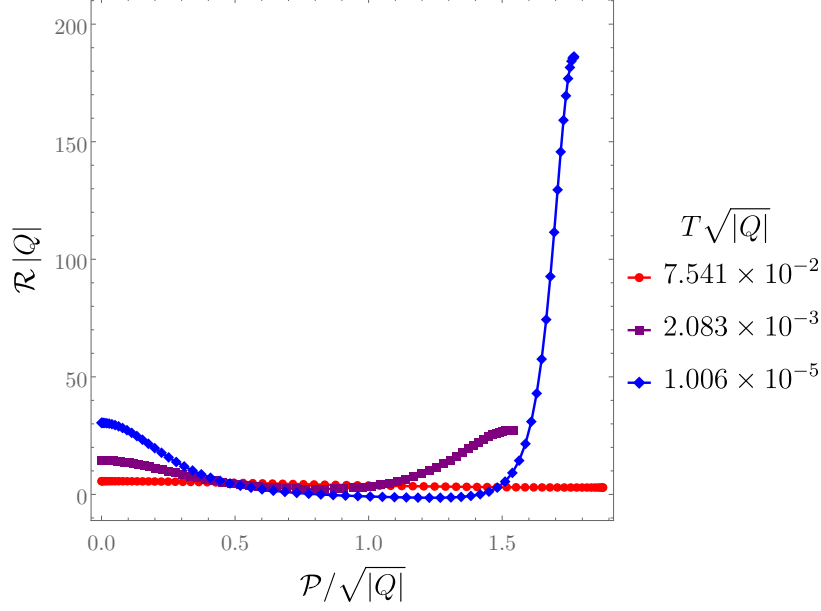


Figure 12. The normalised Ricci scalar $\mathcal{R}|Q|$ as a function of the normalised proper distance from the ψ axis $\mathcal{P}/\sqrt{|Q|}$ at fixed $\lambda = 3/2$, $J_\psi/J_\phi = 3/8$ and $J_\phi/|Q|^{3/2} = 8/(5\sqrt{\pi})$. The normalised temperatures are labelled on the right.

Finally, to gain further insight into the behavior of the local geometry of the spatial horizon cross-sections, we create a parametric plot of $R_\phi, R_\psi/\sqrt{|Q|}$ along spatial cross-sections of the horizon, with $\lambda = 3/2$, $J_\psi/J_\phi = 3/8$ and $J_\phi/|Q|^{3/2} = 8/(5\sqrt{\pi})$ held constant, across various temperatures. This is shown in the left panel of Fig. 13. As the temperature decreases, the horizon adopts a spindle shape, with high curvature concentrated at the spindle’s tip. We also monitored the electric charge density, ρ_e , defined as the pullback of $\star F + \frac{\lambda}{\sqrt{3}}F \wedge A$ onto spatial cross-sections of the horizon, normalised by the volume element of the spatial cross-sections. Even though there is no charged matter, the Chern-Simons term provides an effective charge density as shown in Eq. (2.3). The right panel of Fig. 13 shows the normalised charge density $\rho_e\sqrt{|Q|}$, revealing a region of negative charge density within the spindle, while near the axis generated by $\partial/\partial\psi$, a concentration of positive charge density is observed.

6 Discussion

We have explored the extremal limit of the generic 5D (asymptotically flat) rotating charged black hole, and found a number of surprises. Perhaps the most important is the fact that the horizon becomes singular. In Einstein-Maxwell theory, curvature scalars remain finite at the extremal horizon, but infalling observers see diverging electric fields and experience diverging tidal forces. We have also shown that “general relativity knows about supergravity” in the sense that if one adds a Chern-Simons term and increases its coefficient λ , this singularity remains until one reaches the supergravity value $\lambda = 1$. The extremal horizon is smooth for

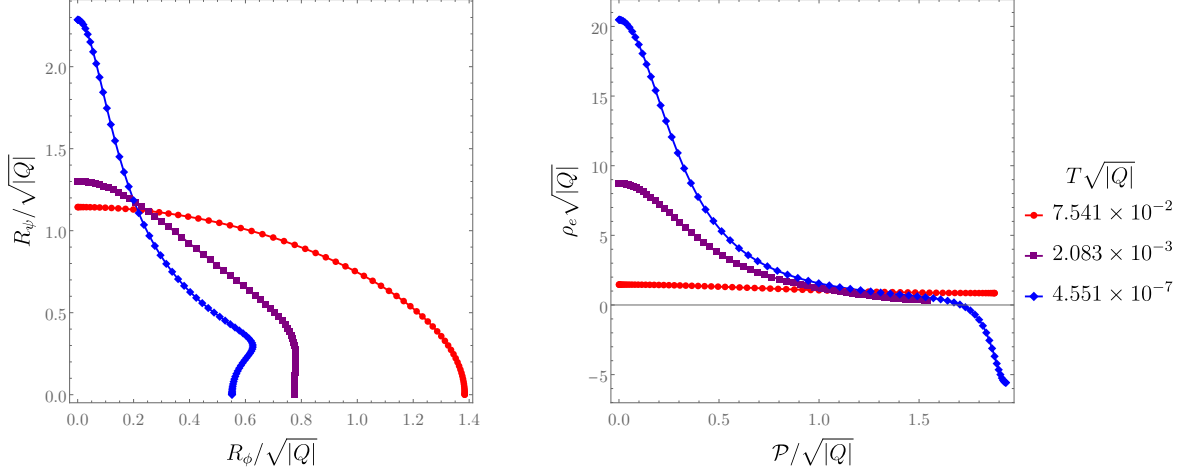


Figure 13. *Left panel.* Parametric plot of $R_\phi, R_\psi/\sqrt{|Q|}$ along spatial cross-sections of the horizon. *Right panel.* Normalised charge density, $\rho_e \sqrt{|Q|}$ (as defined in the main text), plotted as a function of the normalised proper distance, $\mathcal{P}/\sqrt{|Q|}$. Both panels are generated with $\lambda = 3/2$, $J_\psi/J_\phi = 3/8$ and $J_\phi/|Q|^{3/2} = 8/(5\sqrt{\pi})$, with various temperatures indicated on the right.

this one value of λ , but for $\lambda > 1$ the singularity becomes stronger and even curvature scalars diverge.

Another surprise concerns the limit of vanishing angular momenta. We found that this limit depends on the ratio J_ϕ/J_ψ as both angular momenta are scaled to zero. One approaches the 5D Reissner-Nordström solution only when $J_\phi/J_\psi = 1$. In general, one approaches a new family of static, extremal black holes which are not spherically symmetric. One can view this as a form of spontaneous breaking of spherical symmetry. The limiting black hole is static and asymptotically flat, so there is nothing preventing it from being spherically symmetric. Since the scaling dimensions computed in Appendix A are all integers, these new solutions probably have smooth horizons⁹. It is easy to construct nonspherical static extremal black holes when there is more than one horizon (since there is no force between the black holes) and it is known that 5D black holes are not uniquely characterized by their asymptotic charges, but this is different. It is a new form of nonuniqueness for a single extremal 5D black hole.

We have also studied generic near-extremal black holes and shown that the tidal forces are anomalously large but finite. They diverge only in the extremal limit. If one starts with a near extremal black hole, the double limit of approaching extremality and turning off the angular momenta depends on the order of limits. If one first removes the angular momenta, the result is always the spherical Reissner-Nordström solution. As we just discussed, the opposite order yields a nonspherical solution.

The fact that extremal black holes have smooth horizons just for the Chern-Simons coefficient required for supergravity might lead one to wonder if extremal black holes in

⁹The noninteger scaling dimensions computed in Sec. 4.1 correspond to vector modes which are not sourced in the static, asymptotically flat solution.

supergravity will always have smooth horizons. It is easy to see that this is not the case. The Myers-Perry solution with only one nonzero angular momentum has a singular extremal limit, even though it is a solution of minimal 5D supergravity. Perhaps a better question is whether *supersymmetric* black holes in supergravity always have smooth extremal limits. However the answer is still no. The BMPV solution [32] is a well known supersymmetric black hole and has a smooth horizon. But multi-BMPV solutions exist which are still supersymmetric and have tidal force singularities on the horizons [33, 34].

We have focussed on five-dimensional black holes, but we expect that generic extremal black holes in higher dimensions will also have singular horizons. (There is no extremal limit if some angular momenta vanish, but that is not the generic situation.) In fact the singularities are likely to be worse, since that is what happens in AdS for extremal black holes with perturbed boundary conditions [7, 35]. Recalling that even in 4D general relativity, extremal black holes have singular horizons as soon as any higher derivative correction is included [5, 6], the lesson is that smooth extremal horizons are the exception and not the rule.

Acknowledgments

It is a pleasure to thank Maciek Kolanowski for collaboration at an early stage of this work. G.H. was supported in part by NSF Grant PHY-2408110. J.E.S. has been partially supported by STFC consolidated grant ST/X000664/1. G.H. and J.E.S. were also supported in part by grant NSF PHY-2309135 to the Kavli Institute for Theoretical Physics (KITP) where this work was begun.

A Scaling dimensions of the $U(1) \times U(1)$ symmetric near-horizon geometries

In this appendix we compute the scaling dimensions of the static $U(1) \times U(1)$ symmetric near-horizon geometries given in Eq. (3.4). As discussed in section 4.1, the linear equations that determine the scaling dimensions decouple into three groups G_1, G_2, G_3 (4.4). Define

$$S_p(x) \equiv {}_2F_1(-p, p+1; 1; x^2) \quad \text{with } p \geq 0. \quad (\text{A.1})$$

We find three families of modes in G_1 with $\gamma \geq 1$. The first family is given by

$$\begin{aligned} \gamma &= p-1, \quad \text{with } p \geq 2, \\ q_1^{(0)}(x) &= -2pS_p(x) + \frac{x}{\sigma(x)} (1-x^2) (c_1 - c_2) S'_p(x), \\ q_3^{(0)}(x) &= -2p(1+p) (1-2x^2) S_p(x) + \frac{x}{2\sigma(x)} [4(1+p) (1-x^2) \sigma(x) - c_2] S'_p(x), \\ q_4^{(0)}(x) &= 2p(1+p) (1-2x^2) S_p(x) + \frac{(1-x^2)}{2x\sigma(x)} [c_1 - 4(1+p)x^2\sigma(x)] S'_p(x), \\ q_8^{(0)}(x) &= S_p(x). \end{aligned} \quad (\text{A.2})$$

The second family is given by

$$\begin{aligned}
\gamma &= p, \quad \text{with } p \geq 1, \\
q_1^{(0)}(x) &= \frac{x}{\sigma(x)} (1-x^2) (c_1 - c_2)^2 S'_p(x), \\
q_3^{(0)}(x) &= 2p(1+p) (c_1 + c_2) S_p(x) - x \left[1 + \frac{c_1 - c_2}{2\sigma(x)} \right] c_2 S'_p(x), \\
q_4^{(0)}(x) &= -2p(1+p) (c_1 + c_2) S_p(x) - (1-x^2) \left[1 + \frac{c_2 - c_1}{2\sigma(x)} \right] c_1 \frac{S'_p(x)}{x}, \\
q_8^{(0)}(x) &= S_p(x).
\end{aligned} \tag{A.3}$$

Finally, the third family is given by

$$\begin{aligned}
\gamma &= p+1, \quad \text{with } p \geq 0, \\
q_1^{(0)}(x) &= 2(1+p) S_p(x) + \frac{x(1-x^2)}{\sigma(x)} (c_1 - c_2) S'_p(x), \\
q_3^{(0)}(x) &= -2p(1+p) (1-2x^2) S_p(x) - x \left[\frac{c_2}{2\sigma(x)} + 2p(1-x^2) \right] S'_p(x), \\
q_4^{(0)}(x) &= 2p(1+p) (1-2x^2) S_p(x) + (1-x^2) \left[\frac{c_1}{2\sigma(x)} + 2px^2 \right] \frac{S'_p(x)}{x}, \\
q_8^{(0)}(x) &= S_p(x).
\end{aligned} \tag{A.4}$$

For deformations in G_2 we find

$$q_5^{(0)}(x) = {}_2F_1(-p, p+3; 2; x^2) \quad \text{with } \gamma = p+1. \quad \text{where } p \geq 0. \tag{A.5}$$

Note that the scaling dimensions γ are integers for all of these modes.

The remaining sector, i.e. G_3 , is discussed in the main text as well as the modes with $\gamma = 0$.

B The scaling dimensions of the near-horizon geometries of extremal Myers-Perry black holes

In this appendix we compute the general scaling dimensions associated to the near-horizon limit of extremal Myers-Perry black holes. We will assume throughout that $\gamma^{(0)} \neq 0$ (note that modes with $\gamma^{(0)} = 0$ were discussed in section 4.2), and show that γ is always a positive integer, consistent with earlier results in the literature [23, 25]. Unlike modes with $\gamma^{(0)} = 0$, modes with $\gamma^{(0)} \neq 0$ only decouple in two groups:

$$G_1 = \{z_1^{(0)}, z_2^{(0)}, z_3^{(0)}, z_4^{(0)}, z_5^{(0)}, z_6^{(0)}, z_7^{(0)}\} \quad \text{and} \quad G_2 = \{z_8^{(0)}, z_9^{(0)}, z_{10}^{(0)}\}. \tag{B.1}$$

We will describe first the modes in G_2 , as these are substantially simpler to write. Set

$$H_1(x) \equiv x^2 + 4\Omega_\phi^2, \quad H_2(x) \equiv x^2 + 4\Omega_\phi^2(1-x^2). \tag{B.2}$$

and

$$S_p(x) = {}_2F_1(-p, p+1; 1; x^2) . \quad (\text{B.3})$$

We find three families of modes, given by

$$\begin{aligned} \gamma^{(0)} &= p-1 \quad \text{with} \quad p \geq 2 \\ z_8^{(0)}(x) &= \frac{1}{(p-1)\Omega_\phi H_1(x)} \left\{ -2pH_2(x)S_p(x) + x \left[H_2(x) + 2\Omega_\phi^2 - \frac{1}{2} \right] S'_p(x) \right\} , \\ z_9^{(0)}(x) &= -\frac{4\Omega_\phi}{(p-1)H_2(x)} \left\{ 2pH_2(x)S_p(x) + (1-x^2) [H_2(x) - 2\Omega_\phi^2] \frac{S'_p(x)}{x} \right\} , \\ z_{10}^{(0)}(x) &= S_p(x) , \end{aligned} \quad (\text{B.4})$$

$$\begin{aligned} \gamma^{(0)} &= p \quad \text{with} \quad p \geq 1 \\ z_8^{(0)}(x) &= -\frac{x}{2p\Omega_\phi H_1(x)} (1 + 4\Omega_\phi^2) S'_p(x) \\ z_9^{(0)}(x) &= \frac{8(1-x^2)\Omega_\phi^3}{pH_2(x)} \frac{S'_p(x)}{x} \\ z_{10}^{(0)}(x) &= S_p(x) \end{aligned} \quad (\text{B.5})$$

and

$$\begin{aligned} \gamma^{(0)} &= p+1 \quad \text{with} \quad p \geq 0 \\ z_8^{(0)}(x) &= \frac{1}{\Omega_\phi H_1(x)} \left\{ 2H_2(x)S_p(x) + \frac{x}{2(p+1)} [2H_2(x) + 4\Omega_\phi^2 - 1] S'_p(x) \right\} \\ z_9^{(0)}(x) &= 4\Omega_\phi \left\{ 2S_p(x) - \frac{(1-x^2)}{(p+1)H_2(x)} [H_2(x) - 2\Omega_\phi^2] \frac{S'_p(x)}{x} \right\} \\ z_{10}^{(0)}(x) &= S_p(x) \end{aligned} \quad (\text{B.6})$$

In G_1 , the equations are substantially harder to solve. Nevertheless, we identified five families of modes, matching the expected number of families based on this symmetry ansatz and the order of the differential equations being solved. Before presenting the modes, we will first describe a few generalities.

So long as $\gamma^{(0)} \neq 0, 1$, the Einstein equation demands

$$z_7^{(0)}(x) = -\frac{3}{2}z_1^{(0)}(x) - \frac{1}{2}z_2^{(0)}(x) - \frac{1}{2}z_4^{(0)}(x) . \quad (\text{B.7})$$

For $\gamma^{(0)} = 1$ we impose the above as gauge condition, since modes with $\gamma^{(0)} = 1$ exhibit a residual gauge symmetry similar to the one found in [6].

An additional component of the Einstein equation implies

$$\begin{aligned}
z_3^{(0)}(x) = & \frac{H_1(x) [H_2(x) + 4\Omega_\phi^2]}{8x\Omega_\phi^2 H_2(x)} \left\{ - \frac{3H_3^+(x)H_3^-(x)H_2(x)}{x^3(1-x^2) [H_2(x) + 4\Omega_\phi^2]} z_1^{(0)}(x) \right. \\
& + \frac{H_2(x)H_4(x)}{x^3(1-x^2) H_1(x) [H_2(x) + 4\Omega_\phi^2]} z_2^{(0)}(x) + \frac{H_2(x)(H_2(x) - 2x^4)}{x^3(1-x^2)(x^2 + 4\Omega_\phi^2)} z_4^{(0)}(x) - \frac{1}{\gamma^{(0)}} z_6^{(0)'}(x) \\
& \left. + \frac{H_2(x)^2}{x^2 [H_2(x) + 4\Omega_\phi^2]} [3z_1^{(0)'}(x) + z_2^{(0)'}(x) + z_4^{(0)'}(x)] - \frac{4(1-x^2)\Omega_\phi^2 [H_2(x) + 1]}{x^2 [H_2(x) + 4\Omega_\phi^2] \gamma^{(0)}} z_5^{(0)'}(x) \right\},
\end{aligned} \tag{B.8}$$

with

$$\begin{aligned}
H_3^\pm(x) &\equiv x^2 \pm 2\Omega_\phi(1-x^2), \\
H_4(x) &\equiv 16\Omega_\phi^4 - 48\Omega_\phi^4 x^2 - (1 + 12\Omega_\phi^2 - 32\Omega_\phi^4)x^4 - (1 - 4\Omega_\phi^2)x^6.
\end{aligned} \tag{B.9}$$

At this stage we are left with solving for $\{z_1^{(0)}(x), z_2^{(0)}(x), z_4^{(0)}(x), z_5^{(0)}(x), z_6^{(0)}(x)\}$. These all obey second order equations of motion, and we thus expect five degrees of freedom to emerge.

One of these degrees of freedom can be decoupled via the following change of variables

$$\begin{aligned}
z_1^{(0)}(x) &= \frac{1}{3} [h_T(x) - z_2^{(0)}(x) - z_4^{(0)}(x)], \\
z_2^{(0)}(x) &= r_1(x) - r_2(x) - x^4 h_T(x) + x^3(1-x^2)h_T'(x), \\
z_4^{(0)}(x) &= r_2(x) - (1-x^2+2x^4)h_T(x) - (1-2x^2)x(1-x^2)h_T'(x) \\
z_5^{(0)}(x) &= r_3(x) + \frac{\Theta_1(x)}{8(\gamma^{(0)}+1)(1+4\Omega_\phi^2)\Omega_\phi^2} h_T(x) + \frac{\Theta_2(x)}{16(\gamma^{(0)}+1)(1+4\Omega_\phi^2)\Omega_\phi^2} x(1-x^2)h_T'(x) \\
z_6^{(0)}(x) &= r_4(x) + \frac{\Theta_3(x)}{2(\gamma^{(0)}+1)(1+4\Omega_\phi^2)} h_T(x) + \frac{\Theta_4(x)}{4(\gamma^{(0)}+1)(1+4\Omega_\phi^2)} x(1-x^2)h_T'(x)
\end{aligned} \tag{B.10}$$

with

$$\begin{aligned}
\Theta_1(x) &\equiv 4\Omega_\phi^2 - 8x^2\Omega_\phi^2 - x^4 [1 - 8(2 - \lambda^{(0)})\Omega_\phi^2 - 16(3 - 2\lambda^{(0)})\Omega_\phi^4] \\
\Theta_2(x) &\equiv 4\Omega_\phi^2 + x^2(1 - 16\Omega_\phi^2 - 48\Omega_\phi^4) \\
\Theta_3(x) &\equiv 3 + (4 + 8\lambda^{(0)})\Omega_\phi^2 - 16(3 - 2\lambda^{(0)})\Omega_\phi^4 - x^2 [6 + 8\Omega_\phi^2 - 96\Omega_\phi^4 - 4\lambda^{(0)}(1 - 16\Omega_\phi^4)] \\
&\quad + x^4 [5 + 16\Omega_\phi^2 - 48\Omega_\phi^4 - 4\lambda^{(0)}(1 + 2\Omega_\phi^2 - 8\Omega_\phi^4)] \\
\Theta_4(x) &\equiv 3 + 4\Omega_\phi^2 - 48\Omega_\phi^4 - x^2(5 + 16\Omega_\phi^2 - 48\Omega_\phi^4)
\end{aligned} \tag{B.11}$$

where $\lambda^{(0)} \equiv \gamma^{(0)}(\gamma^{(0)} + 1)$.

The equation for h_T decouples from the remainder four equations for r_1, r_2, r_3 and r_4 , and can be readily solved via

$$h_T(x) = {}_2F_1(-p, p+3; 2; x^2) \quad \text{with} \quad \gamma^{(0)} = p+1 \quad p \geq 0. \tag{B.12}$$

We are left with solving for r_1 , r_2 , r_3 and r_4 , which all couple and obey linear second order differential equations with variable coefficients.

It turns out that these four equations can be solved exactly and solutions fall into four classes which we now detail.

In the first family

$$\begin{aligned}
\gamma^{(0)} &= p \\
r_1(x) &= pS_1(x), \\
r_2(x) &= \frac{1 + 4\Omega_\phi^2}{H_1(x)} \left[px^2 S_1(x) + \frac{x(1-x^2)}{2(p+1)} S_1'(x) \right], \\
r_3(x) &= \frac{1}{8(p+1)\Omega_\phi^2} \left\{ -pH_2(x)S_1(x) \right. \\
&\quad \left. + \frac{x}{2(p+1)} [(p^2 + p + 1) H_2(x) - 1 + 4p(1+p)\Omega_\phi^2] S_1'(x) \right\}, \\
r_4(x) &= \frac{1}{8(p+1)} \left\{ -4pH_2(x)S_1(x) \right. \\
&\quad \left. + \frac{2}{p+1} [(p^2 + p + 1) H_2(x) - 4\Omega_\phi^2 + p^2 + p] \frac{(1-x^2)S_1'(x)}{x} \right\},
\end{aligned} \tag{B.13}$$

with $S_1(x) \equiv {}_2F_1(-p, p+1; 1; x^2)$, where $p \geq 1$.

In the second family

$$\begin{aligned}
\gamma^{(0)} &= p \\
r_1(x) &= x^2 S_2(x), \\
r_2(x) &= \frac{2x^2(x^2 + 2\Omega_\phi^2)}{3(x^2 + 4\Omega_\phi^2)} S_2(x), \\
r_3(x) &= -\frac{\Omega_\phi^2}{3(p+1)(1 + 4\Omega_\phi^2)} [2S_2(x) + x(1 - 2x^2) S_2'(x)], \\
r_4(x) &= -\frac{1}{12(p+1)(1 + 4\Omega_\phi^2)} [2S_2(x) + x(1 - 2x^2) S_2'(x)],
\end{aligned} \tag{B.14}$$

with $S_2(x) \equiv {}_2F_1(-p, p+1; 2; x^2)$, where $p \geq 1$.

In the third family

$$\begin{aligned}
\gamma^{(0)} &= p + 1 \\
r_1(x) &= \frac{x^6 \gamma^{(0)}}{H_2(x)} S_3(x), \\
r_2(x) &= \frac{2}{3} \frac{x^6 \gamma^{(0)}}{H_2(x)} S_3(x) \\
r_3(x) &= -\frac{x^4(p+1)}{12(p+2)(1+4\Omega_\phi^2)} \left[\frac{6\Omega_\phi^2 + x^2(1-2\Omega_\phi^2)}{(1-x^2)\Omega_\phi^2} S_p(x) + x S'_p(x) \right], \\
r_4(x) &= \frac{1}{3(2+p)^2(1+4\Omega_\phi^2)} \left[\varpi_1(x) S_3(x) + \frac{x}{2} S'_p(x) \right].
\end{aligned} \tag{B.15}$$

with $S_3(x) \equiv {}_2F_1(-p, p+3; 4; x^2)$, where $p \geq 0$ and

$$\begin{aligned}
\varpi_1(x) &= 4x^4(1+\Omega_\phi^2) - 3(1+4\Omega_\phi^2) - p(p+3)x^2[1+4\Omega_\phi^2 - 2x^2(1+\Omega_\phi^2)], \\
\varpi_2(x) &= 2(p+1)(p+2)x^4(1+2\Omega_\phi^2) - p(p+3)x^2(1+4\Omega_\phi^2) - 2 - 8\Omega_\phi^2.
\end{aligned} \tag{B.16}$$

Finally, for the fourth family we find

$$\begin{aligned}
\gamma^{(0)} &= p \\
r_1(x) &= \frac{x^4}{H_2(x)} S_4(x), \\
r_2(x) &= \frac{2}{3} \frac{x^4}{H_2(x)} S_4(x) \\
r_3(x) &= \frac{x^5}{48(1-x^2)(p+1)\Omega_\phi^2} S'_4(x), \\
r_4(x) &= -\frac{1}{3(p+1)} \left[S_4(x) + \frac{x(1-x^2)}{4} S'_4(x) \right].
\end{aligned} \tag{B.17}$$

with $S_4(x) \equiv {}_2F_1(-p, p+1; 3; x^2)$, where $p \geq 1$.

References

- [1] F. R. Tangherlini, “Schwarzschild field in n dimensions and the dimensionality of space problem,” *Nuovo Cim.* **27** (1963) 636–651.
- [2] R. C. Myers and M. J. Perry, “Black Holes in Higher Dimensional Space-Times,” *Annals Phys.* **172** (1986) 304.
- [3] Z. W. Chong, M. Cvetič, H. Lu, and C. N. Pope, “General non-extremal rotating black holes in minimal five-dimensional gauged supergravity,” *Phys. Rev. Lett.* **95** (2005) 161301, [arXiv:hep-th/0506029](#).
- [4] R. Deshpande and O. Lunin, “Rotating Einstein-Maxwell black holes in odd dimensions,” [arXiv:2411.01795 \[hep-th\]](#).

- [5] G. T. Horowitz, M. Kolanowski, G. N. Remmen, and J. E. Santos, “Extremal Kerr Black Holes as Amplifiers of New Physics,” *Phys. Rev. Lett.* **131** no. 9, (2023) 091402, [arXiv:2303.07358 \[hep-th\]](#).
- [6] G. T. Horowitz, M. Kolanowski, G. N. Remmen, and J. E. Santos, “Sudden breakdown of effective field theory near cool Kerr-Newman black holes,” *JHEP* **05** (2024) 122, [arXiv:2403.00051 \[hep-th\]](#).
- [7] G. T. Horowitz, M. Kolanowski, and J. E. Santos, “Almost all extremal black holes in AdS are singular,” *JHEP* **01** (2023) 162, [arXiv:2210.02473 \[hep-th\]](#).
- [8] H. K. Kunduri and J. Lucietti, “Static near-horizon geometries in five dimensions,” *Class. Quant. Grav.* **26** (2009) 245010, [arXiv:0907.0410 \[hep-th\]](#).
- [9] J. L. Blázquez-Salcedo, J. Kunz, and F. Navarro-Lerida, “Angular momentum - area - proportionality of extremal charged black holes in odd dimensions,” *Phys. Lett. B* **727** (2013) 340–344, [arXiv:1309.2088 \[gr-qc\]](#).
- [10] A. Komar, “Covariant conservation laws in general relativity,” *Phys. Rev.* **113** (1959) 934–936.
- [11] D. N. Page, “Classical Stability of Round and Squashed Seven Spheres in Eleven-dimensional Supergravity,” *Phys. Rev. D* **28** (1983) 2976.
- [12] K. Hanaki, K. Ohashi, and Y. Tachikawa, “Comments on charges and near-horizon data of black rings,” *JHEP* **12** (2007) 057, [arXiv:0704.1819 \[hep-th\]](#).
- [13] H. K. Kunduri and J. Lucietti, “Classification of near-horizon geometries of extremal black holes,” *Living Rev. Rel.* **16** (2013) 8, [arXiv:1306.2517 \[hep-th\]](#).
- [14] J. M. Bardeen, B. Carter, and S. W. Hawking, “The Four laws of black hole mechanics,” *Commun. Math. Phys.* **31** (1973) 161–170.
- [15] B. Carter, “Killing horizons and orthogonally transitive groups in space-time,” *J. Math. Phys.* **10** (1969) 70–81.
- [16] S. W. Hawking, “Black hole explosions,” *Nature* **248** (1974) 30–31.
- [17] H. K. Kunduri, J. Lucietti, and H. S. Reall, “Near-horizon symmetries of extremal black holes,” *Class. Quant. Grav.* **24** (2007) 4169–4190, [arXiv:0705.4214 \[hep-th\]](#).
- [18] M. Cvetič and D. Youm, “General rotating five-dimensional black holes of toroidally compactified heterotic string,” *Nucl. Phys. B* **476** (1996) 118–132, [arXiv:hep-th/9603100](#).
- [19] M. Headrick, S. Kitchen, and T. Wiseman, “A New approach to static numerical relativity, and its application to Kaluza-Klein black holes,” *Class. Quant. Grav.* **27** (2010) 035002, [arXiv:0905.1822 \[gr-qc\]](#).
- [20] T. Wiseman, *Numerical construction of static and stationary black holes*, pp. 233–270. Cambridge University Press, 2012. [arXiv:1107.5513 \[gr-qc\]](#).
- [21] O. J. C. Dias, J. E. Santos, and B. Way, “Numerical Methods for Finding Stationary Gravitational Solutions,” *Class. Quant. Grav.* **33** no. 13, (2016) 133001, [arXiv:1510.02804 \[hep-th\]](#).
- [22] P. Figueras and T. Wiseman, “On the existence of stationary Ricci solitons,” *Class. Quant. Grav.* **34** no. 14, (2017) 145007, [arXiv:1610.06178 \[gr-qc\]](#).

- [23] M. Durkee and H. S. Reall, “Perturbations of near-horizon geometries and instabilities of Myers-Perry black holes,” *Phys. Rev. D* **83** (2011) 104044, [arXiv:1012.4805 \[hep-th\]](#).
- [24] J. Kunz and F. Navarro-Lerida, “D=5 Einstein-Maxwell-Chern-Simons black holes,” *Phys. Rev. Lett.* **96** (2006) 081101, [arXiv:hep-th/0510250](#).
- [25] K. Murata, “Instability of higher dimensional extreme black holes,” *Class. Quant. Grav.* **30** (2013) 075002, [arXiv:1211.6903 \[gr-qc\]](#).
- [26] G. Carullo, D. Laghi, N. K. Johnson-McDaniel, W. Del Pozzo, O. J. C. Dias, M. Godazgar, and J. E. Santos, “Constraints on Kerr-Newman black holes from merger-ringdown gravitational-wave observations,” *Phys. Rev. D* **105** no. 6, (2022) 062009, [arXiv:2109.13961 \[gr-qc\]](#).
- [27] O. J. C. Dias, M. Godazgar, J. E. Santos, G. Carullo, W. Del Pozzo, and D. Laghi, “Eigenvalue repulsions in the quasinormal spectra of the Kerr-Newman black hole,” *Phys. Rev. D* **105** no. 8, (2022) 084044, [arXiv:2109.13949 \[gr-qc\]](#).
- [28] A. Davey, O. J. C. Dias, P. Rodgers, and J. E. Santos, “Strong Cosmic Censorship and eigenvalue repulsions for rotating de Sitter black holes in higher-dimensions,” *JHEP* **07** (2022) 086, [arXiv:2203.13830 \[gr-qc\]](#).
- [29] O. J. C. Dias, M. Godazgar, and J. E. Santos, “Eigenvalue repulsions and quasinormal mode spectra of Kerr-Newman: an extended study,” *JHEP* **07** (2022) 076, [arXiv:2205.13072 \[gr-qc\]](#).
- [30] A. Davey, O. J. C. Dias, and J. E. Santos, “Scalar QNM spectra of Kerr and Reissner-Nordström revealed by eigenvalue repulsions in Kerr-Newman,” *JHEP* **12** (2023) 101, [arXiv:2305.11216 \[gr-qc\]](#).
- [31] A. Davey, O. J. C. Dias, and D. S. Gil, “Strong Cosmic Censorship in Kerr-Newman-de Sitter,” *JHEP* **07** (2024) 113, [arXiv:2404.03724 \[gr-qc\]](#).
- [32] J. C. Breckenridge, R. C. Myers, A. W. Peet, and C. Vafa, “D-branes and spinning black holes,” *Phys. Lett. B* **391** (1997) 93–98, [arXiv:hep-th/9602065](#).
- [33] G. N. Candlish and H. S. Reall, “On the smoothness of static multi-black hole solutions of higher-dimensional Einstein-Maxwell theory,” *Class. Quant. Grav.* **24** (2007) 6025–6040, [arXiv:0707.4420 \[gr-qc\]](#).
- [34] G. N. Candlish, “On the smoothness of the multi-BMPV black hole spacetime,” *Class. Quant. Grav.* **27** (2010) 065005, [arXiv:0904.3885 \[hep-th\]](#).
- [35] G. T. Horowitz, M. Kolanowski, and J. E. Santos, “A deformed IR: a new IR fixed point for four-dimensional holographic theories,” *JHEP* **02** (2023) 152, [arXiv:2211.01385 \[hep-th\]](#).